Engineering properties of vertical cutoff walls consisting of reactive magnesia-activated slag and bentonite: Workability, strength and hydraulic conductivity

Hao-Liang Wu
Ph.D. Student, Jiangsu Key Laboratory of Urban Underground Engineering & Environmental Safety, Institute of Geotechnical Engineering, Southeast University, Nanjing 210096, China. Email: 230149672@seu.edu.cn

Fei Jin
Assistant Professor, School of Engineering, University of Glasgow, Glasgow G12 8QQ, UK. Email: fei.jin@glasgow.ac.uk (Co-first author with equal contribution)

Jin Ni
Graduate Student, Jiangsu Key Laboratory of Urban Underground Engineering & Environmental Safety, Institute of Geotechnical Engineering, Southeast University, Nanjing 210096, China. Email: 220162700@seu.edu.cn

Yan-Jun Du*
Professor, Jiangsu Key Laboratory of Urban Underground Engineering & Environmental Safety, Institute of Geotechnical Engineering, Southeast University, Nanjing 210096, China. Tel.: +862583793729; Fax: +862583795086,
*Corresponding author, Email: duyanjun@seu.edu.cn

Revised Manuscript Submitted to

Journal of Materials in Civil Engineering

Abstract

The soil-cement-bentonite (SCB) vertical cutoff walls are commonly used to control flow of contaminated groundwater in polluted sites. However, conventional backfill consisting of Ordinary Portland cement (OPC) is associated with relatively high CO_2 footprint. Potential chemical interactions between OPC and bentonite could also undermine the long-term durability of SCB materials. In this paper, we propose an innovative backfill material for cutoff walls, which is composed of MgO-activated ground granulated blast furnace slag (GGBS), bentonite and soil. The OPC-soil, OPC-bentonite-soil, and OPC-GGBS–bentonite-soil backfill materials are also tested for comparison purpose. Workability of the fresh backfills and unconfined compressive strength of aged backfills are investigated. The hydraulic conductivities of aged backfills permeated with tap water, Na_2SO_4 and Pb-Zn solutions are assessed. The unconfined compressive strength and hydraulic conductivity of the proposed backfill permeated with tap water for the backfills are in the range of 230 - 520 kPa and 1.1×10^{-10} - 6.3×10^{-10} m/s at 90-day-curing, respectively, depending on the mix composition. The hydraulic conductivity of the proposed MgO-GGBS-bentonite-soil backfill permeated with sodium sulfate (Na_2SO_4) or lead-zinc (Pb-Zn) solution is well below the commonly used limit, while the OPC-bentonite-soil backfill shows a significant loss in its impermeability. Environmental and economic analyses indicate that, compared with the conventional backfill made from the OPC-bentonite-soil mixture, the proposed backfill reduces approximately 84.7% - 85.1% in CO_2 emissions and 15.3% - 16.9% cost. The environmental and economic advantages will

promote the utilization of MgO-activated GGBS-bentonite mixtures in the cutoff walls and further advocate its application in land remediation projects.

Keywords: Cutoff wall; reactive MgO-activated GGBS; unconfined compressive strength; hydraulic conductivity

Introduction

The low-permeability and cost-effective cutoff walls have been widely used in the remediation projects for various contaminated sites in the world (Ryan and Day 2002; Shen et al. 2013; Shen et al. 2017; Yang et al. 2018). They have been mainly used to interrupt the pollution pathway and isolate the contaminant source from a vulnerable receptor (Joshi et al. 2008; Soga and Joshi 2015). Depending on the backfill materials, cutoff walls can be classified as soil-bentonite (SB), cement-bentonite (CB) and soil-cement-bentonite (SCB) (Du et al. 2015; Opdyke and Evans 2005). SCB walls have gained more popularity in some regions since the strength of SB walls may be inadequate to carry foundation loads (Opdyke and Evans 2005). In addition, compared with CB walls, the reuse of site excavated soils in SCB walls provide additional economic merits, as the discarded soil would create additional transportation and disposal expenditure (Ryan and Day 2002). Currently, Ordinary Portland cement (OPC) is the dominant cement used in SCB and CB walls. However due to its negative engineering and environmental impacts (e.g., large CO_2 emissions and consumption of raw materials (Jin and Al-Tabbaa 2014a; Wu et al. 2018a; Xu et al. 2019), several industrial by-products including but not limited to ground granulated blast furnace slag (GGBS) have been widely used in land remediation and ground improvement practice (Arulrajah et al. 2016; Arulrajah et al. 2018; Kua et al. 2016; Maghool et al. 2016; Liu et al. 2019; Du et al. 2019). For example, GGBS has been successfully used to partially substitute cement in the low permeability cutoff walls (Jefferis 2012). The recently developed geopolymer also can

79 be potentially applied to cutoff walls as an innovative construction material (Arulrajah
80 et al. 2017a; Arulrajah et al. 2017b; Lam and Jefferis 2017).

81 The most important engineering properties of SCB walls are unconfined
82 compressive strength (usually in the range of 100 - 700 kPa) and hydraulic
83 conductivity (within 5.0×10^{-9} - 1.0×10^{-8} m/s at 28-day-curing) (Ryan and Day 2002).
84 When OPC is added to the bentonite suspension, hydration occurs, forming primary
85 cementitious products, namely calcium silicate hydrate (C-S-H), ettringite, and
86 portlandite ($Ca(OH)_2$, CH) (Carreto et al. 2015; Ryan and Day 2002). The released
87 calcium (Ca^{2+}) ions from the hydrated products replace the monovalent cation, e.g.,
88 sodium (Na^{+}), which are held on the exchangeable sites of bentonite particles, leading
89 to the flocculation of bentonite (Cuisinier et al. 2008; Gaucher and Blanc 2006).
90 Furthermore, the high pH environment facilitates the dissolution of the inherent
91 silicate and aluminate sheets in the bentonite structure, leading to the formation of
92 secondary cementitious materials, i.e., C-S-H and calcium aluminate hydrate (C-A-H)
93 in the matrix of mixtures. On one hand, these secondary cementitious materials
94 enhance the bonding between solid particles to provide higher strength and better
95 filling of pore space (Carreto et al. 2015). On the other hand, the stability and swelling
96 properties of bentonite could be significantly undermined. The instability of bentonite
97 soils under high pH conditions created by PC has been extensively studied in the
98 radioactive waste encapsulation projects, which leads to the use of low-pH materials
99 to achieve a better compatibility with bentonite and thus higher long-term durability
100 (Cuisinier et al. 2008; Gaucher and Blanc 2006; Sánchez et al. 2006).

Reactive MgO-activated GGBS is a recently developed binder which produces C-S-H, hydrotalcite and brucite ($Mg(OH)_2$, if MgO is excessive) upon hydration (Du et al. 2016; Jin et al. 2015; Jin and Al-Tabbaa 2014a; Wang et al. 2016). Due to the lack of highly soluble portlandite, this material can be potentially used as a low pH and durable binder, which offers a range of geomechanical and geoenvironmental advantages over OPC in land remediation projects (Jin et al. 2015; Jin et al. 2016; Jin and Al-Tabbaa 2014a; Wang et al. 2019). The contaminant binding capability, sulfate resistance and wetting-drying durability of MgO-activated GGBS have been studied in recent years (Du et al. 2016; Jin and Al-Tabbaa 2014a; Wu et al. 2018a). However, its application in cutoff walls has not been explored yet while it is anticipated that it will have better compatibility with bentonite than OPC as shown above.

This paper aims to describe the performance of a more cost-effective and sustainable cutoff wall backfill material by utilizing MgO-activated GGBS-bentonite-soil mixtures. A systematic mix design procedure is implemented to investigate the engineering properties including workability, unconfined compressive strength and hydraulic conductivity permeated with tap water, Na_2SO_4 and Pb-Zn solutions respectively. Environmental and cost analyses are also performed and compared with the conventional OPC-based backfill mixtures.

Materials and Testing Methods

Constituent materials

The materials used for preparation of the backfill in this study consisted of

123 Nanjing local clayey sand, powdered bentonite and cementitious materials (i.e., OPC,
124 MgO and GGBS). The physicochemical properties of Nanjing local clayey sand and
125 commercial powdered sodium activated calcium-bentonite used in this study are
126 shown in **Table 1**. Due to the low availability of high-quality Na-bentonite in China,
127 sodium activated calcium-bentonite is used in this study, which was proved to be a
128 good alternative in vertical cutoff walls (Jefferis 2012; Yang et al. 2018). The
129 powdered bentonite was provided by MuFeng mineral processing plant in Zhenjiang
130 City, China.

131 The constituent materials, including Ordinary Portland cement (OPC) class 42.5,
132 GGBS and MgO, were both obtained from Nanjing, China. The reactivity of MgO
133 was ~ 102 s, determined by the acetic acid test according to Shand (2006). Based on
134 the characteristic by Jin and Al-Tabbaa (2014a), the reactive MgO was categorized as
135 a medium reactivity MgO, which was selected due to its appropriate reactivity and
136 cost (Jin et al. 2015; Jin and Al-Tabbaa 2014a; Wu et al. 2018a). **Table 2** shows the
137 chemical compositions of Nanjing local clayey sand, OPC, GGBS and MgO used for
138 this study.

139

140 **Mix design guideline**

141 The investigation methodology for the backfills consisted of three main steps, as
142 illustrated in **Fig. 1**. Step 1 was used to evaluate the workability of backfill materials
143 for the cutoff wall. Step 2 was composed of four sub-steps to select binder and binder
144 content based on relative demand for hydraulic conductivity, unconfined compressive

145 strength, chemical compatibility and sustainability performance. Therefore, the final
146 binder proportion was obtained from the system. The mix proportions are based on
147 review of previous studies including both field and lab test results of SCB cutoff walls
148 (**Fig. S1**). For SCB backfill, the hydraulic conductivity commonly used in
149 contaminant containment systems is suggested to be no higher than 1×10^{-8} m/s (Ryan
150 and Day 2002). A target of 100 kPa was set as the minimum unconfined compressive
151 strength for SCB cutoff wall in recent projects as suggested by previous researchers
152 (BRE 1999; Ryan and Day 2002).
153
154 **Specimens preparation and testing methods**
155 Four categories of binders, namely OPC (Ref), OPC-bentonite (CB),
156 OPC-GGBS-bentonite (CSB) and MgO-GGBS-bentonite (MSB), were mixed with
157 clayey sand at room temperature (20 ± 2^{o}C) in a 2-L Hobart stainless steel mixer to
158 form backfills. The content of the GGBS used in the OPC-GGBS-bentonite system
159 was 80% replacement of OPC, which was reported to exhibit the lowest hydraulic
160 conductivity and highest strength (Opdyke and Evans 2005). The MgO to GGBS ratio
161 in the MgO-GGBS-bentonite system was 1:9 to achieve good strength based on
162 preliminary studies (Jin et al. 2015; Jin et al. 2016). The mixing procedure consists of
163 three steps: 1) solid ingredients, including clayey sand, OPC, bentonite, GGBS and
164 MgO, were weighted according to mix proportions presented in **Table 3**; 2) solid
165 ingredients were homogeneously mixed at 30 rpm for 5 min; and 3) a predetermined
166 amount of tap water (pH = 6.8; *EC* = 3.3 μS/cm) was added and then mixed at 60 rpm

for 10 min to achieve homogeneous mixtures.

With the selected binder combinations, slump test was conducted to evaluate the workability of backfills. The fresh backfills immediately subjected to the slump test should have a slump value ranging between 100 mm and 200 mm in order to achieve the optimum workability (Ryan and Day 2002). In this study a target slump value of 150 ± 5 mm was selected to prepare backfills. A mini-slump was conducted together with the standard slump test as described by Malusis et al. (2008).

The fresh backfill with the target slump values was prepared to conduct the unconfined compressive strength and hydraulic conductivity tests. The unconfined compressive strength was performed in triplicate according to ASTM D4219 (ASTM 2008) at a constant loading rate of strain of 1%/min after curing for 14, 28, 60, 90 and 120 days. The crushed specimens after curing 28 and 90 days were ground and mixed with distilled water (water to solid ratio = 1: 1) to determine the pore water pH according to Jin et al. (2015). The pH value was measured in triplicate using a pH meter HORIBA D-54 and the average value was reported. The hydraulic conductivity permeated with tap water (k_w) was conducted on specimens after 28 and 90 days of curing using the flexible-wall permeameters. These specimens were fully saturated for 23 ± 0.5 hours by applying a vacuum pressure of 80 kPa before being assembled into the permeameters. During the permeation, the tap water was applied from lower base to the upper side of the specimen under the seepage pressure in order to avoid air entrapment. The cell pressure and a constant flow pressure were respectively set as 200 kPa and 150 kPa, which were lower than the yield stress of the specimens. It is

noted that volume change was found to be negligible during the tests, because the yield stress (σ_y') of the specimens was estimated to be in the range of 201 - 1428 kPa based on the relationship of σ_y' = 1.4 - 2.2 q_u for OPC stabilized soil proposed by Horpibulsuk et al. (2004). During the permeating, the ambient temperature was strictly controlled at 22 ± 2 °C. Based on ASTM D5084 (ASTM 2016), the termination criteria of k_w were achieved when: 1) the ratio of outflow to inflow was within 0.75 – 1.25; 2) the hydraulic conductivity is steady, namely, the hydraulic conductivity versus time showed no significant upward or downward trend. The hydraulic conductivity shall be considered steady if four or more consecutive hydraulic conductivity determinations fall within ±25 % or better of the mean value for $k \geq 1\times10^{-10}$ m/s or within ±50 % or better for $k \leq 1\times10^{-10}$ m/s (ASTM 2016).

The hydraulic conductivity permeated with Na_2SO_4 or Pb-Zn solution was also assessed immediately after permeating with tap water for the specimens cured for 90 days. The test was continued by replacing the tap water with Na_2SO_4 or Pb-Zn solution as the permeant liquid, and the hydraulic conductivity (k_c) was determined as per ASTM D7100 (ASTM 2011). Sulfates significantly affect the integrity and hydraulic conductivity of cutoff walls by attacking the cement in CB and SCB cutoff walls (Garvin and Hayles 1999). Garvin and Hayles (1999) chose the Na_2SO_4 (30 mmol/L, pH = 7.82) solution as a representative sulfate source to observe the deterioration of cutoff walls upon sulfate attack. The target Na_2SO_4 solution (30 mmol/L) was prepared by dissolving predetermined weight of $Na_2SO_4{\cdot}10H_2O$ powder (chemical analytical reagent) in distilled water. The Pb-Zn solution (pH = 6.51,

concentration of Pb = 0.1 mg/L and Zn = 5 mg/L) was prepared with distilled water, lead nitrate ($Pb(NO_3)_2$) and zinc nitrate solution ($Zn(NO_3)_2 \cdot 10H_2O$) power (chemical analytical reagent). Pb and Zn were selected as simulation contamination sources as they are commonly encountered in groundwater in abandoned battery and mining fields (Cao et al. 2009; Du et al. 2015; Rodríguez et al. 2009; Xia et al. 2019a and 2019b; Yang et al. 2019). The Pb and Zn concentrations set in this study are the maximum values of groundwater quality Grade IV prescribed by the Ministry of Ecology and Environment of the People's Republic of China. Hong et al. (2017) also used Zn (5 mg/L) in their research exploring the transport of Zn across backfill specimens. The hydraulic conductivity permeated with Na_2SO_4 or Pb-Zn solution was assessed by ASTM D7100 (ASTM 2011). The termination criteria for the chemical equilibrium is reached when 1) ratio of outflow volume to inflow volume are within 0.75 -1.25; 2) the solute concentration, pH, electrical conductivity (*EC*) and/or dielectric constant of outflow are within ± 10% of those of inflow, and 3) there is insignificant variation of these abovementioned parameters. The sulfate ion concentration was measured using a Thermos Scientific^{TM} Dionex Ion Chromatography. The value of *EC* and concentrations of Pb and Zn were measured using an Orion 4-Star Plus pH/Conductivity Benchtop Multiparameter Meter and inductively coupled plasma optical emission spectrometry (ICP-OES), respectively.

Results and Analysis

Workability

Fig. 2 (a) presents the variation of standard slump value (S_s) with mini-slump

234 value (S_m) for all the mixtures listed in **Table 3**. It is observed that there is a positive
235 correlation between the two values for all backfills. The empirical relationship can be
236 adequately represented by a single linear expression and well agree with Malusis et al.
237 (2008) as shown in **Eq. 1**. It indicates that the mini-slump test can be used to predict
238 the standard slump value for the backfills satisfactorily.

239 $$S_s = 2S_m + 49,\ R^2 = 0.96 \quad (1)$$

240 A plot of S_s versus water content for each mixture is illustrated in **Fig. 2 (b)**. It is
241 evident that S_s increases approximately linearly with water content as increasing water
242 content in the backfills induces lower density and yield stress (Cheng et al. 2018). The
243 linear fitting equations of S_s versus water content are summarized in **Table 4**. The
244 measured values of density and water content for all fresh backfill materials at the
245 target slump values are also shown in **Table 4**.

246

247 **Unconfined compressive strength and failure strain**

248 **Fig. 3 (a)** shows the evolution of unconfined compressive strength (q_u) for the
249 four categories of backfill specimens. The strength gain of the OPC-based specimens
250 is mainly attributed to cement hydration, which is fast and becomes plateaued after
251 ~28 days. Herein the q_u for Ref, CB and CSB backfill specimens achieve 520 - 650
252 kPa and 530 - 680 kPa at 28-day and 90-day curing, respectively. In contrast, the
253 strength development of the MSB system is relatively slow and only after 90 days the
254 strength appeared to stabilize at ~230 - 520 kPa. For the identical MgO-activated
255 GGBS content, it is found that increasing bentonite content slightly reduced the

strength of MSB mixtures which is probably due to the higher water content and lower dry density as achieved the approximately same workability (see **Table 4**). Although the q_u of MSB backfill specimens is lower than that of the OPC-based ones, it is clear that all the mixtures satisfied the q_u requirement after curing for 28-day (≥ 100 kPa (BRE 1999; Ryan and Day 2002)). **Fig. 3 (b)** shows the failure strain (ε_f) for the four categories of backfill specimens. As compared to OPC-based specimens, the failure strains of MSB backfill specimens are 33.0 - 47.6% and 16.6 - 31.2 % higher at 28-day and 90-day curing, respectively. A regression analysis is conducted for identifying the correlation between failure strain and strength. It can be seen that the failure strain tends to decrease as the strength increases.

pH value and dry density

Fig. 4 illustrates the variation of pH values with curing time for the backfill specimens except for MS5B5 whose pH value at 90-day-curing is only slightly lower than that at 28-day-curing. For all the specimens, pH gradually increased slightly with curing time, indicating the continuation of the hydration reactions. It can be seen that the pH values of the OPC-based backfill are ~ 11.7 - 12.4 after 90 days of curing, which is much than those of MSB backfills (10.1 - 10.8).

The dry density and void ratio of backfill specimens after curing 28 days and 90 days are summarized in **Table 5**. The increase of the dry density is more noticeable in MSB backfill specimens as compared to Ref, CB and CSB, which is consistent with the q_u evolution as shown in **Fig. 3**.

278

279 **Hydraulic conductivity permeated with tap water**

280 The evolution of k_w with curing time is displayed in **Fig. 5**. The slightly
281 decreased k_w from 28 days to 90 days is observed in CB and CSB. Conversely, the k_w
282 values of MSB show a pronounced decrease by 0.4 - 0.8 orders of magnitude as
283 curing time increases from 28 days to 90 days. The k_w is higher than commonly
284 accepted limit (1.0×10^{-8} m/s) suggested by Ryan and Day (2002) for the OPC-soil
285 (Ref) and C5B5 cured at 28 days, while those of the CSB and MSB are much lower
286 than the commonly accepted limit, regardless of the curing time. Increasing the binder
287 dosage slightly reduces the k_w for all the mixtures. For example, k_w is decreased by 52%
288 when MgO-activated GGBS is increased from 5% to 10% at 90 days (2.3×10^{-10} m/s
289 for MS5B15 vs. 1.1×10^{-10} m/s for MS10B15). On the other hand, increasing bentonite
290 dosage from 5% to 10% in MSB backfill specimens at 90 days reduces k_w by ~63%
291 (6.3×10^{-10} m/s vs. 2.3×10^{-10} m/s).

292

293 **Chemical equilibrium**

294 **Fig. 6** shows the variation of volumetric flow ratio, pH and *EC* ratio, and
295 consternation ratio with pore volumes of flow (*PVF*) as permeated with Na_2SO_4 and
296 Pb-Zn solution. As presented in **Fig. 6 (a)** and **(b)**, the maximum, average and
297 minimum value of volumetric flow ratio (Q_{out}/Q_{in}) for the test are within 0.75 - 1.25
298 before and after permeated with Na_2SO_4 or Pb-Zn solution. It indicates that the
299 hydraulic equilibrium was established by the end of trial. **Fig. 6 (c)** shows the pH and

300 *EC* equilibrium status of the outflow and inflow for all backfill materials permeated
301 with Na_2SO_4. The pH and *EC* in the effluents slightly and gradually decrease with the
302 increasing *PVF*. The values of pH_{out}/pH_{in} and EC_{out}/EC_{in} are both within the target
303 range of 0.9 and 1.1, and therefore pH and *EC* equilibrium have been reached at the
304 end of test as permeated with Na_2SO_4. When permeated with Pb-Zn solution, the
305 results of pH and *EC* equilibrium status for all backfill materials show consistent
306 trends as permeated with Na_2SO_4 (**Fig. 6 (d)**). Some values of pH_{out}/pH_{in} are out of
307 the target range of 0.9 and 1.1, but the values of EC_{out}/EC_{in} fall within. As shown in
308 **Fig. 6 (e) – (f)**, the concentration ratio of SO_4^{2-}, Pb and Zn concentration increases
309 steadily after approximately 2.2 -2.4 *PVF*. Based on the results shown in **Fig. 6 (b) –**
310 **(f)**, the chemical equilibrium was reached at the end of trail termination.

311

312 **Hydraulic conductivity permeated with Na_2SO_4 and Pb-Zn solution**

313 **Fig. 7** illustrates the hydraulic conductivity of specimens permeated with tap
314 water (k_w), Na_2SO_4 and Pb-Zn (k_c) as well as the ratio between the two values (k_c/k_w).
315 It is apparent that the MSB backfill specimens show lower hydraulic conductivity
316 than Ref, CB and CSB backfill specimens, regardless of the permeation liquid. For the
317 MSB, k_c decreases by 13% - 57% when permeated with Na_2SO_4 solution as compared
318 to k_w permeated with tap water. In contrast, Na_2SO_4 solution significantly increases
319 the hydraulic conductivities by one to two magnitudes for the Ref and CB and 1 - 2
320 times for the CSB. When permeated with the Pb-Zn solution, the k_c of all the backfill

materials increases, with those OPC-based ones (Ref, CB and CSB) even by 1 - 2 magnitudes while MSB only by 2 - 5 times. When the bentonite dosage increases from 5% to 15% in the MSB systems, the k_c/k_w decreases by 28.7% and 40.9% for the Na_2SO_4 and Pb-Zn cases, respectively. On the other hand, k_c/k_w decreases by 55.7% and 27.0% as the MgO-activated GGBS dosage increases from 5% to 10% for the Na_2SO_4 and Pb-Zn cases, respectively.

Environmental impact and cost analyses

To quantify the environmental and economic impact of the proposed cutoff wall backfill materials, two major indicators, CO_2 emissions and economic cost are chosen (Wu et al. 2018b), which are collected for each component as shown in **Table 6**. The cost of each component is summarized in the average price provided by multiple suppliers in Nanjing city (China) market in 2018. The calculation for CO_2 emission and cost for cutoff wall backfills can be expressed as:

$$T_{CO_2,j} = \rho_d \sum_{i=1}^{n} \left(\frac{m_i}{m_j} \times F_{CO_2,i}\right) \quad (2)$$

$$T_{cost,j} = \rho_d \sum_{i=1}^{n} \left(\frac{m_i}{m_j} \times F_{cost,i}\right) \quad (3)$$

where: $T_{CO_2,j}$ and $T_{cost,j}$ refer to the total CO_2 emissions and cost of code j (indicating the backfill type), (GJ/m^3), respectively; ρ_j is the dry density of code j obtained from **Table 4**, (t/m^3); m_i and m_j are the mass of component i and total mass in code j obtained from **Table 3**, (t), respectively; $F_{CO_2,i}$ and $F_{cost,i}$ are the CO_2 emissions and cost of component i obtained from **Table 6**, (GJ/ m^3), respectively.

342 **Table 7** shows the net CO_2 emissions and materials' cost for the backfill
343 materials. It can be seen that the substituting OPC with GGBS significantly improves
344 the sustainability performance (comparing C5B5 and CS5B5). Compared to CB
345 backfill, the CSB and MSB backfill materials have 78.7% - 79.3% and 84.7% - 85.1%
346 less CO_2 emissions, and 9.3% -12.5% and 15.3% - 16.9% less cost, respectively.
347 When the bentonite dosage increases for the same type of binder (5% in MS5B5 vs.
348 15% in MS5B15), cost increases by 50.8% but CO_2 emission decreases by 24.3% due
349 to the higher water content of MSB system associated to achieve the same workability
350 (see **Table 4**). On the other hand, increasing the MgO-activated GGBS dosage (5% in
351 MS5B10 vs. 10% in MS10B10) increases the CO_2 emissions and cost by 90.4% and
352 27.2%, respectively. In practice, however, the cost and environmental impacts not
353 only depend on the materials used but also are significantly associated with the
354 contamination source and construction methods (Ryan and Day 2002). In this study,
355 MSB mixtures show superior environmental benefits while possessing desirable
356 technical properties as alternative cutoff wall backfill materials.
357
358 **Discussion**
359 The mechanisms controlling the variations of unconfined compressive strength
360 and hydraulic conductivity in each category of the backfill materials are summarized
361 as follows:
362 1) OPC hydration is fast, gaining most of the strength within 28 days of curing.
363 Although high strength and low cost can be achieved with OPC alone as the backfill

binder, the hydraulic conductivity does not satisfy the commonly accepted limit (1×10^{-8} m/s) and the carbon footprint is higher when using the material and methods described earlier. Adding bentonite to the OPC-soil mixture slightly decreases the q_u, significantly increases the cost, but meanwhile reduces the hydraulic conductivity (Ref vs. C5B5). In addition, it is noted that at 28 days of curing, increasing the OPC and bentonite dosage from 5% to 10% decreases k_w of CB backfill specimens by 2 times (1.2×10^{-8} m/s vs. 5.8×10^{-9} m/s); however, at 90 days of curing, only marginal improvement on hydraulic performance (8.7×10^{-9} m/s vs. 4.7×10^{-9} m/s) is observed. As the OPC-GGBS and bentonite dosages increase from 5% to 10%, the hydraulic performance of CSB exhibits negligible improvement at 28 days of curing (5.9×10^{-9} m/s vs. 4.8×10^{-9} m/s), whereas it decreases by 2 - 4 times after 90 days of curing (~1.3 $\times10^{-9}$ m/s - 3.1 $\times10^{-9}$ m/s). Overall, OPC and C5B5 system are not recommended for cutoff wall backfill considering their inadequate technical (i.e., k_c higher than 1×10^{-8} m/s for Ref and C5B5 backfill specimens) and environmental performance (i.e., higher net CO_2 emission and costs for CB system). Replacing OPC with GGBS as the binder in the cutoff wall backfill has been applied extensively in the UK (Shand 2006; Jefferis 2012). It imparts significant environmental and economic benefits, marginally affects the q_u (sometimes with enhancement), slightly decreases pH and notably decreases hydraulic conductivity in the long term (**Fig. 5**). GGBS reacts with portlandite in hydrated OPC to produce C-S-H, which lowers the pH and improves the strength and hydraulic performance. Nevertheless, the pH in CSB system is still high (~11.3 - 11.9 at 28 - 90 days curing) (**Fig. 4**)) to react with bentonite, leading to the

386 breakage of aluminate and silicate sheets to some extent (Cuisinier et al. 2008;
387 Sánchez et al. 2006). In addition, Ca and Al ions released from OPC and GGBS
388 hydration products and/or bentonite in the pore water of CSB backfills, which would
389 further react with sulfate ions when the backfill specimens is exposed to sodium
390 sulfate solution to produce expansive ettringite and gypsum, generating inner pressure
391 and damage CSB backfill matrix (Jefferis 2012; Müllauer et al. 2013), which was
392 manifested with higher k_c permeated with Na_2SO_4 solution than k_w permeated with tap
393 water for CSB backfill specimens (**Fig. 7**).

394 2) pH has a significant impact on the chemical stability of montmorillonite in
395 bentonite (Cuisinier et al. 2008; Jefferis 2012; Sánchez et al. 2006). In order to fully
396 utilize the binding properties of the binders to enhance the strength and the swelling
397 properties of the bentonite to achieve commonly accepted hydraulic conductivity of
398 the cutoff wall, the pore fluid pH of MSB backfill systems should be explored. MSB
399 backfill specimens develop q_u much slower due to its lower pH relative to CSB
400 backfill specimens. Nevertheless, q_u of MSB backfill specimens continues to develop
401 over time (**Fig. 3**) due to the formation of C-S-H and Ht, leading to denser
402 microstructure (Carreto et al. 2015; Ryan and Day 2002; Ma et al. 2019) and
403 consequently lower hydraulic conductivity in the long term compared to the CSB
404 backfill specimens. In addition, there is a lack of free portlandite in the MSB backfill
405 specimens, which leads to a much lower pore fluid pH (10.0 to 10.7 at 28-day-curing
406 and 10.1 to 10.8 at 90 days of curing (**Fig. 4**) as compared to CSB backfill specimens
407 (11.3 to 11.6 at 28 days of curing and 11.7 to 11.9 at 90 days of curing (**Fig. 4**). The

408 higher pH in CSB system could accelerate the attack of aluminate and silicate sheets
409 of bentonite by the OH^- (Savage et al. 2007). Meanwhile, the released Ca from OPC
410 and GGBS would replace Na^+ at the exchangeable sites of bentonite particles due to
411 higher replaceability of Ca^{2+} than that of Na^+, resulting increased hydraulic
412 conductivity of bentonite. The aforementioned attack of aluminate and silicate sheets
413 of bentonite and ion exchange reaction tend to reduce the swelling potential of
414 bentonite and increase the k_w of the CSB backfill (Dauzeres et al. 2010). On the other
415 hand, MSB mixtures showed much lower pore fluid pH as shown in **Fig. 4,** which
416 imparts smaller adverse impacts on the swelling potential of bentonite, resulting in
417 marginal change in k_w (**Fig. 5**).

418 3) Less calcium ions in the MSB system also means the formation of expansive
419 gypsum and ettringite can be effectively limited, which has been proved in (Yi et al.
420 2014) where only C-S-H, Ht and a small amount of ettringite were observed in
421 MgO-GGBS paste exposed to Na_2SO_4 solution. Excessive formation of ettringite can
422 produce high expansive force to crack the matrix leading to spalling and higher
423 hydraulic conductivity (Cai et al. 2014; Neville 2004). On the other hand, a small
424 amount of ettringite helps to densify the matrix instead of causing cracks, which is
425 demonstrated by the lower k_c of MSB backfill specimens as compared to the k_c of
426 CSB backfill specimens permeated with Na_2SO_4 solution (**Fig. 7**). In addition, the
427 presence of sulfate would accelerate hydration of GGBS, forming more C-S-H
428 products in the MSB backfill specimens (Provis 2014) , which contributes to the fact
429 that k_c/k_w is lower than 1.0 (**Fig. 7**). Whereas, the pozzolanic reaction of OPC could

430 be significantly retarded by the presence of Pb and Zn, imposing adverse effects on
431 the microstructure, leaving relatively a large amount of macro-pores in the matrix (Du
432 et al. 2014; Zhou et al. 2016), which would also contribute to the higher k_c of the CB
433 and CSB backfill materials. However, compared to CB and CSB backfill, the
434 influence of Pb-Zn solution on the k_c is much smaller for MSB backfill due to the
435 high adsorption capacity of Pb and Zn by Ht (Jin and Al-Tabbaa 2014b), one of the
436 main hydration products formed in the MgO-GGBS mixture matrix, and thus
437 mitigates the adverse effect of Pb and Zn on the swelling potential and hydraulic
438 conductivity of bentonite.

439 Admittedly that for a full understanding of the mineralogical and microstructural
440 evolution of the MSB backfills before and after permeating with Na_2SO_4 and Pb-Zn
441 solutions, microstructural analyses are warranted. Further, future work should also be
442 conducted on the sulfate-soaking tests and integrity analyses in order to address how
443 and how much different sulfate sources (e.g., $MgSO_4$) would attack OPC-based and
444 MSB backfill specimens differently. Furthermore, the cone penetration test with pore
445 pressure readings (CPTu) is warranted to measure unconfined compressive strength
446 and hydraulic conductivity of in-site vertical cutoff walls (Manassero 1994; Li et al.
447 2019).

448

449 **Limitations of current study**

450 Generally, the SCB backfills in various lab-scale tests can be prepared by the
451 following two methods: (1) mixing prehydrated bentonite slurry (bentonite-water)

452 with in-site soil-OPC mixture (Opdyke and Evans 2005; Ryan and Day 2002).
453 Additional dry bentonite can be added to the soil-cement-bentonite mixture to reach
454 the target slump height (Ryan and Day 2002), and (2) mixing OPC- water grout
455 (weight ratio = 1: 1) with in-site soil and prehydrated bentonite slurry (Ruffing and
456 Evans 2014). Nevertheless, neither method can prevent the attack of high pH of OPC
457 to the bentonite or cation exchange reactions between free cations (e.g., Ca^{2+}) in the
458 hydrated OPC and readily exchangeable cations in the bentonite (e.g., Na^{+}). It is
459 reported that when partially GGBS-replaced OPC was added to bentonite, less
460 flocculation of bentonite was observed, and lower hydraulic conductivity of the
461 cement-bentonite cutoff wall backfills could be achieved (Jefferis 2012). In this study,
462 the backfill specimens subjected to various hydraulic conductivity tests were prepared
463 by mixing the non-prehydrated bentonite with sandy soil-OPC mixture. This could
464 explain the higher hydraulic conductivity of the C5B5 mixture (**Fig. 5**) than the
465 commonly accepted limit. Moreover, the non-prehydrated bentonite that deviates from
466 the field practice may result in different hydraulic conductivities between the
467 laboratory and field results. It is reported that prehydration of bentonite can reduce
468 hydraulic conductivity of GCLs permeated with tap water by two or three times
469 (Shackelford and Sample-Lord 2014; Young Jo et al. 2004). Nonetheless, we
470 demonstrate that the proposed backfill with the non-prehydrated bentonite lab-scale
471 tests could possess lower hydraulic conductivity (k_c and k_w) than the commonly
472 accepted limit.

473 The superior performance of this novel cutoff wall backfill material could be
474 attributed to the much lower pH value of its pore water compared to OPC-bentonite or
475 OPC-GGBS-bentonite mixture (**Fig. 4**). Further studies are suggested to investigate
476 the effects of pore water chemistry of MgO-GGBS on the flocculation and swelling
477 potential of bentonite. Furthermore, it is recognized that the hydraulic conductivity
478 measured after 2 - 4 *PVF* may not be able to assess the long-term performance of SCB
479 walls (Shackelford and Jefferis 2000), hence long term equilibrium should be
480 established in further studies. It is warranted to prepare the backfill specimens using
481 sufficiently pre-hydrated bentonite and investigate their hydraulic performance in the
482 lab-scale and field-scale tests.
483

484 **Conclusions**

485 This study demonstrates that the innovative MgO-GGBS-bentonite system can
486 serve as an alternative backfill for cutoff walls, providing satisfactory workability and
487 unconfined compressive strength, superior hydraulic conductivity performance and
488 remarkable environmental benefits. Based on the experimental results, the following
489 conclusions can be drawn:

490 (1) The mini-slump test could be used to predict the standard slump value for the
491 MgO-GGBS-bentonite-soil and OPC-based backfill materials satisfactorily due to the
492 good positive correlation between the two test values.

493 (2) The MgO-GGBS-bentonite-soil backfill materials showed pH range from
494 10.0 - 10.7 at 28-day-curing and 10.1 -10.8 at 90-day-curing, which were lower than

the OPC-based backfill ranging from 11.3 - 11.8 and 11.7 - 12.4 at 28 and 90-day-curing, respectively.

(3) The unconfined compressive strength for the MgO-GGBS-bentonite-soil backfill reached 140 - 280 kPa and 230 - 520 kPa at the corresponding curing age. The unconfined compressive strength of OPC-based backfill developed 2.0% - 10.3% but the MgO-GGBS-bentonite-soil backfill continued to develop 70.2% - 86.1% after 28-day-curing.

(4) The hydraulic conductivity permeated with tap water for the OPC-based backfill was 1 - 2 magnitudes higher than MgO-GGBS-bentonite-soil backfill at 28-day-curing and 90-day-curing. In addition, the MgO-GGBS-bentonite-soil backfill binder could achieve 8.5×10^{-10} - 4.2×10^{-9} m/s and 1.1×10^{-10} - 6.3×10^{-10} m/s at 28-day-curing and 90-day-curing, respectively.

(5) The proposed MgO-GGBS-bentonite-soil backfill exhibited hydraulic conductivity of 4.7×10^{-11} - 5.5×10^{-10} m/s and 2.3×10^{-10} – 2.9×10^{-9} m/s when permeated with Na_2SO_4 and Pb-Zn solutions, respectively. In contrast, the hydraulic conductivity of OPC-based backfill permeated with Na_2SO_4 and Pb-Zn solutions was one to two magnitudes higher than that of the MgO-GGBS-bentonite-soil backfill.

(6) Environmental and economic benefits could be achieved by utilizing the proposed MgO-GGBS-bentonite-soil backfill, resulting in 84.7% - 85.1% less CO_2 emissions and 15.3% - 16.9% less cost as compared to the OPC-bentonite-soil backfill.

Acknowledgments

This study is finanically supported by National Key Research and Development Programme (Grant No. 2018YFC1803100 and 2018YFC1802300), National Natural Science Foundation of China (Grant No. 41877248), Primary Research & Development Plan of Jiangsu Province (Grant No. BE2017715), the Colleges and Universities in Jiangsu Province Plans to Graduate Research and Innovation (KYLX16_0242), and the Scientific Research Foundation of Graduate School of Southeast University (Grant No. YBJJ1735). The first author is supported by a grant from the Chinese Scholarship Council as a visiting scholar at the University of Michigan.

References

Arulrajah, A., A. Mohammadinia, I. Phummiphan, S. Horpibulsuk, and W. Samingthong. 2016. "Stabilization of recycled demolition aggregates by geopolymers comprising calcium carbide residue, fly ash and slag precursors." *Constr. Build. Mater.* 114: 864-873. https://doi.org/10.1016/j.conbuildmat.2016.03.150

Arulrajah, A., T. Kua, S. Horpibulsuk, M. Mirzababaei, and A. Chinkulkijniwat. 2017a. "Recycled glass as a supplementary filler material in spent coffee grounds geopolymers." *Constr. Build. Mater.* 151: 18-27. https://doi.org/10.1016/j.conbuildmat.2017.06.050

Arulrajah, A., T. Kua, C. Suksiripattanapong, S. Horpibulsuk, and J. S. Shen. 2017.

"Compressive strength and microstructural properties of spent coffee grounds-bagasse ash based geopolymers with slag supplements." *J. Clean Prod.* 162: 1491-1501. https://doi.org/10.1016/j.jclepro.2017.06.171

Arulrajah, A., M. Yaghoubi, M. M. Disfani, S. Horpibulsuk, M. W. Bo, and M, Leong. 2018. "Evaluation of fly ash-and slag-based geopolymers for the improvement of a soft marine clay by deep soil mixing." *Soils Found.* 58 (6): 1358-1370. https://doi.org/10.1016/j.sandf.2018.07.005

ASTM. 2008. *Standard test method for unconfined compressive strength index of chemical-grouted soils.* ASTM D4219. West Conshohocken, PA: ASTM.

ASTM. 2010a. *Standard Test Methods for Laboratory Determination of Water (Moisture) Content of Soil and Rock by Mass.* ASTM D2216. West Conshohocken, PA: ASTM.

ASTM. 2010b. *Standard Test Methods for Liquid Limit, Plastic Limit, and Plasticity Index of Soils.* ASTM D4318, West Conshohocken, PA: ASTM.

ASTM. 2010c. *Standard Test Method for Measuring the Exchange Complex and Cation Exchange Capacity of Inorganic Fine-Grained Soils.* ASTM D7503. West Conshohocken, PA: ASTM.

ASTM. 2011. *Standard test methods for hydraulic conductivity compatibility testing of soils with aqueous solutions*. ASTM D4972. West Conshohocken, PA: ASTM.

ASTM. 2014. *Standard Test Methods for Specific Gravity of Soil Solids by Water Pycnometer.* ASTM D4813. West Conshohocken, PA: ASTM,.

ASTM. 2016. *Standard test methods for measurement of hydraulic conductivity of*

saturated porous materials using a flexible wall permeameter. ASTM D5084. West Conshohocken, PA: ASTM.

ASTM. 2018a. *Standard Test Method for pH of Soils*. ASTM D4972. West Conshohocken, PA: ASTM.

ASTM. 2018b. *Standard test methods for laboratory determination of density (unit weight) of soil specimens.* ASTM D7263. West Conshohocken, PA: ASTM.

Cai, G., A. Zhou, and D. Sheng. 2014. "Permeability function for unsaturated soils with different initial densities." *Can. Geotech. J.* 51(12): 1456-1467. https://doi.org/10.1139/cgj-2013-0410

Cao, X., A. L. Ma. Wahbi, B. Li, and Y. Yang, 2009. "Immobilization of Zn, Cu, and Pb in contaminated soils using phosphate rock and phosphoric acid." *J. Hazard. Mater.* 164(2-3): 555-564. https://doi.org/10.1016/j.jhazmat.2008.08.034

Carreto, J. M. R., L. M. M. S. Caldeira, and E. J. L. M. Neves. 2015. "Hydromechanical characterization of cement-bentonite slurries in the context of cutoff wall applications." *J. Mater. Civ. Eng.* 28(2): 04015093. https://doi.org/10.1061/(asce)mt.1943-5533.0001365

Cheng, W., J. C. Ni, J. S. Shen, and Z. Wang. 2018. "Modeling of permeation and fracturing grouting in sand: laboratory investigations." *J. Test. Eval.* 46(5): 2067-2082. https://doi.org/10.1520/jte20170170

Cuisinier, O., F. Masrouri, M. Pelletier, F. Villieras, and R. Mosser-Ruck. 2008. "Microstructure of a compacted soil submitted to an alkaline plume." *Appl. Clay Sci.* 40(1-4): 159-170. https://doi.org/10.1016/j.clay.2007.07.005

583 Dauzeres, A., P. Le Bescop, P. Sardini, and C. C. D. Coumes. 2010.
584 "Physico-chemical investigation of clayey/cement-based materials interaction in the
585 context of geological waste disposal: Experimental approach and results." *Cem.*
586 *Concr. Res.* 40(8): 1327-1340. https://doi.org/10.1016/j.cemconres.2010.03.015
587 Du, Y., N. Jiang, S. Liu, F. Jin, D. N. Singh, and A. J. Puppala. 2014. "Engineering
588 properties and microstructural characteristics of cement-stabilized zinc-contaminated
589 kaolin." *Can. Geotech. J.* 51(3): 289-302. https://doi.org/10.1139/cgj-2013-0177
590 Du, Y., R. Fan, K. R. Reddy, S. Liu, and Y. Yang. 2015. "Impacts of presence of lead
591 contamination in clayey soil – calcium bentonite cutoff wall backfills." *Appl. Clay Sci.*
592 108: 111-122. https://doi.org/10.1016/j.clay.2015.02.006
593 Du, Y., Bo, Y., Jin, F., and Liu, C. 2016. "Durability of reactive magnesia-activated
594 slag-stabilized low plasticity clay subjected to drying – wetting cycle." *Eur. J.*
595 *Environ. Civ. Eng.* 20(2): 215-230. https://doi.org/10.1080/19648189.2015.1030088
596 Du, Y. J., J. Wu, Y. L. Bo, and N. J. Jiang. 2019. "Effects of acid rain on physical,
597 mechanical and chemical properties of GGBS–MgO-solidified/stabilized
598 Pb-contaminated clayey soil." *Acta Geotech.* 1-10.
599 https://doi.org/10.1007/s11440-019-00793-y
600 Garvin, S. L., and C. S. Hayles. 1999. "The chemical compatibility of cement –
601 bentonite cut-off wall material." *Constr. Build. Mater.* 13(6): 329-341.
602 https://doi.org/10.1016/s0950-0618(99)00024-0
603 Gaucher, E. C., and P. Blanc. 2006. "Cement/clay interactions – a review:
604 experiments, natural analogues, and modeling." *Waste Manage.* 26(7): 776-788.

https://doi.org/10.1016/j.wasman.2006.01.027

Hong, C. S., C. D. Shackelford, and M. A. Malusis. 2017. "Numerical evaluation of vertical cutoff walls comprising zeolite-amended backfills for enhanced metals containment." *J. Geotech. Geoenviron. Eng.* 143(7): 04017028. https://doi.org/10.1061/(asce)gt.1943-5606.0001699

Horpibulsuk, S., D. T. Bergado, and G. A. Lorenzo. 2004. "Compressibility of cement-admixed clays at high water content." *Geotechnique*. 54(2): 151-154. https://doi.org/10.1680/geot.54.2.151.36341

ICE (Institution of Civil Engineers). 1999. *Specification for the construction of slurry trench cut-off walls as barriers to pollution migration*. Thomas Telford, London. https://doi.org/10.1680/sftcostcw.26254

Jefferis, S. 2012. "Cement-bentonite slurry systems." *Grouting and deep mixing*, L. F. Johnsen, D. A. Bruce, and M. J. Byle, eds., 1-24. Reston, VA, ASCE. https://doi.org/10.1061/9780784412350.0001

Jin, F., and A. Al-Tabbaa. 2014a. "Characterisation of different commercial reactive magnesia." *Adv. Cem. Res.* 26(2): 101-113. https://doi.org/10.1680/adcr.13.00004

Jin, F., and A. Al-Tabbaa. 2014b. "Evaluation of novel reactive MgO activated slag binder for the immobilization of lead and zinc." *Chemosphere*, 117: 285-294. https://doi.org/10.1016/j.chemosphere.2014.07.027

Jin, F., K. Gu, and A. Al-Tabbaa. 2015. "Strength and hydration properties of reactive MgO-activated ground granulated blastfurnace slag paste." *Cem. Concr. Compos.* 57: 8-16. https://doi.org/10.1016/j.cemconcomp.2014.10.007

627 Jin, F., F. Wang, and A. Al-Tabbaa. 2016. "Three-year performance of in-situ
628 solidified/stabilised soil using novel MgO-bearing binders." *Chemosphere*. 144:
629 681-688. https://doi.org/10.1016/j.chemosphere.2015.09.046
630 Joshi, K., K. Soga, M. Y. A. Ng, and C. Kechavarzi. 2008. "Durability Study of
631 Eleven Years Old Cement-Bentonite Cut-Off Wall Material." *GeoCongress 2008:*
632 *Geotechnics of Waste Management and Remediation*, 620-627. New Orleans, LA,
633 ASCE. https://doi.org/10.1061/40970(309)78
634 Kua, T., A. Arulrajah, S. Horpibulsuk, Y. Du, and S. Shen. 2016. "Strength
635 assessment of spent coffee grounds-geopolymer cement utilizing slag and fly ash
636 precursors." *Constr. Build. Mater.* 115, 565-575.
637 https://doi.org/10.1016/j.conbuildmat.2016.04.021
638 Lam, C., and S. A. Jefferis. 2017. *Polymer Support Fluids in Civil Engineering*, ICE
639 Publishing, One Great George Street, Thomas Telford Limited, London.
640 https://doi.org/10.1680/psfce.57869
641 Li, H., S. Liu, and L. Tong. 2019. "Evaluation of lateral response of single piles to
642 adjacent excavation using data from cone penetration tests." *Can. Geotech. J.* 56(2):
643 236-248. https://doi.org/10.1139/cgj-2018-0131
644 Liu, L., A. Zhou, Y. Deng, Y. Cui, Z. Yu, and C. Yu. 2019. "Strength performance of
645 cement/slag-based stabilized soft clays." *Constr. Build. Mater.* 211, 909-918.
646 https://doi.org/10.1016/j.conbuildmat.2019.03.256
647 Ma, L., D. Xu, S. Wang, and X. Gu. 2019. "Expansion inhibition of steel slag in
648 asphalt mixture by a surface water isolation structure." *Road Mater. Pavement Des.*

649 1-15. https://doi.org/10.1080/14680629.2019.1601588

650 Maghool, F., A. Arulrajah, S. Horpibulsuk, and Y. Du. 2016. "Laboratory evaluation
651 of ladle furnace slag in unbound pavement-base/subbase applications." *J. Mater. Civ.*
652 *Eng.*, 29(2): 04016197. https://doi.org/10.1061/(asce)mt.1943-5533.0001724

653 Malusis, M. A., J. C. Evans, M. H. McLane, and N. R. Woodward. 2008. "A
654 miniature cone for measuring the slump of soil-bentonite cutoff wall backfill."
655 *Geotech. Test. J.* 31(5): 373-380. https://doi.org/10.1520/gtj101487

656 Manassero, M. 1994. "Hydraulic conductivity assessment of slurry wall using
657 piezocone test." *J. Geotech. Eng.* 120(10): 725-1746.
658 https://doi.org/10.1061/(asce)0733-9410(1994)120:10(1725)

659 Müllauer, W., R. E. Beddoe, and D. Heinz. 2013. "Sulfate attack expansion
660 mechanisms." *Cem. Concr. Res.* 52 (2013): 208-215.
661 https://doi.org/10.1016/j.cemconres.2013.07.005

662 Neville, A. 2004. "The confused world of sulfate attack on concrete." *Cem. Concr.*
663 *Res.* 34(8): 1275-1296. https://doi.org/10.1016/j.cemconres.2004.04.004

664 Opdyke, S. M., and J. C. Evans. 2005. "Slag-cement-bentonite slurry walls." *J.*
665 *Geotech. Geoenviron. Eng.* 131(6): 673-681.
666 https://doi.org/10.1061/(asce)1090-0241(2005)131:6(673)

667 Provis, J. L., and J. S. J. van Deventer. 2014. *Alkali Activated Materials. RILEM*
668 *state-of-the-art Reports, RILEM TC 224-AAM.* Springer, Netherlands.
669 https://doi.org/10.1007/978-94-007-7672-2

670 Rodríguez, L., E. Ruiz, J. Alonso-Azcárate, and J. Rincón. 2009. "Heavy metal

671 distribution and chemical speciation in tailings and soils around a Pb‐Zn mine in
672 Spain." *J. Environ. Manage.* 90(2): 1106-1116.
673 https://doi.org/10.1016/j.jenvman.2008.04.007
674 Ruffing, D. G., and J. C. Evans. 2014. “Case Study: Construction and In Situ
675 Hydraulic Conductivity Evaluation of a Deep Soil-Cement-Bentonite Cutoff Wall”. *In*
676 *Proc., Geo-Congress 2014,* 1863-1848. Atlanta, Georgia, ASCE.
677 https://doi.org/10.1061/9780784413272.180
678 Ryan, C. R., and S. R. Day. 2002. "Soil-cement-bentonite slurry walls." *In Deep*
679 *foundations 2002: an international perspective on theory, design,construction, and*
680 *performance (Geotechnical Special Publication).* 713-727.
681 https://doi.org/10.1061/40601(256)51
682 Sánchez, L., J. Cuevas, S. Ramírez, D. R. De León, R. Fernández, R. V. D. Villa, and
683 S. Leguey. 2006. "Reaction kinetics of FEBEX bentonite in hyperalkaline conditions
684 resembling the cement‐bentonite interface." *Appl. Clay Sci.* 33(2): 125-141.
685 https://doi.org/10.1016/j.clay.2006.04.008
686 Savage, D., C. Walker, R. Arthur, C. Rochelle, C. Oda, and H. Takase. 2007.
687 "Alteration of bentonite by hyper alkaline fluids: A review of the role of secondary
688 minerals." *Phys. Chem. Earth.* 32(1-7): 287-297.
689 https://doi.org/10.1016/j.pce.2005.08.048
690 Shackelford, C. D., and S. A. Jefferis. 2000. "Geoenvironmental engineering for in
691 situ remediation" *In Proc. Int. Conf. on Geotech., and Geoenv. Eng.,* GeoEng 2000,
692 121–185, Melbourne, Australia.

693 Shackelford, C. D., and K. M. Sample-Lord. 2014. "Hydraulic conductivity and
694 compatibility of bentonite for hydraulic containment barriers." *Principles and*
695 *practices in geotechnical engineering*, J. Garlanger, M. Hussein, and M. Iskander,
696 eds., 370-387. Reston, VA, ASCE. https://doi.org/10.1061/9780784413265.030
697 Shand, M. A. 2006. *The chemistry and technology of magnesia*, John Wiley & Sons,
698 New Jersey. https://doi.org/10.1002/0471980579
699 Shen, S., L. Ma, Y. Xu, and Z. Yin. 2013. "Interpretation of increased deformation
700 rate in aquifer IV due to groundwater pumping in Shanghai." *Can. Geotech. J.* 50(11):
701 1129-1142. https://doi.org/10.1139/cgj-2013-0042
702 Shen, S.L., Y. Wu, and A. Misra. 2017. "Calculation of head difference at two sides
703 of a cut-off barrier during excavation dewatering." *Comput. Geotech.* 91: 192-202.
704 https://doi.org/10.1016/j.compgeo.2017.07.014
705 Soga, K., and K. Joshi. 2015. "Cement bentonite cutoff walls for polluted sites." *In*
706 *Proc., Coupled Phenomena in Environmental Geotechnics, Taylor & Francis Group,*
707 149-165. https://doi.org/10.1201/b15004-15
708 Wang, F., F. Jin, Z. Shen, and A. Al-Tabbaa. 2016. "Three-year performance of
709 in-situ mass stabilized contaminated site soils using MgO-bearing binders." *J. Hazard.*
710 *Mater.* 318: 302-307. https://doi.org/10.1016/j.jhazmat.2016.07.018
711 Wang, F., J. Xu, and Z. Cai. 2019. "Effects of curing temperature and dosage on the
712 performance of GGBS-MgO-CaO in stabilizing/solidifying heavy metal-contaminated
713 site soil." *J. Test. Eval.* 48(5). https://doi.org/10.1520/jte20180261
714 Wu, H., F. Jin, Y. Bo, Y. Du, and J. Zheng. 2018a. "Leaching and microstructural

715 properties of lead contaminated kaolin stabilized by GGBS-MgO in semi-dynamic
716 leaching tests." *Constr. Build. Mater.* 172: 626-634.
717 https://doi.org/10.1016/j.conbuildmat.2018.03.164
718 Wu, H., D. Zhang, B. R. Ellis, and V. C. Li. 2018b. "Development of reactive
719 MgO-based Engineered Cementitious Composite (ECC) through accelerated
720 carbonation curing." *Constr. Build. Mater.* 191: 23-31.
721 https://doi.org/10.1016/j.conbuildmat.2018.09.196
722 Xia, W. Y., Y. J. Du, F. S. Li, C. P. Li, X. L. Yan, A. Arulrajah, F. Wang, and D. J.
723 Song. 2019a. "In-situ solidification/stabilization of heavy metals contaminated site
724 soil using a dry jet mixing method and new hydroxyapatite based binder." *J. Hazard.*
725 *Mater.* 369: 353-361. https://doi.org/10.1016/j.jhazmat.2019.02.031
726 Xia, W. Y., Y. J. Du, F. S. Li, G. L. Guo, X. L. Yan, C. P. Li, A. Arulrajah, F. Wang,
727 S. Wang. 2019b. "Field evaluation of a new hydroxyapatite based binder for ex-situ
728 solidification/stabilization of a heavy metal contaminated site soil around a Pb-Zn
729 smelter." *Constr. Build. Mater.* 210: 278-288.
730 https://doi.org/10.1016/j.conbuildmat.2019.03.195
731 Yang, Y. L., K. R. Reddy, Y. J. Du, and R. D. Fan. 2018. "Short-term hydraulic
732 conductivity and consolidation properties of soil-bentonite backfills exposed to
733 CCR-impacted groundwater." *J. Geotech. Geoenviron. Eng.* 144(6): 04018025.
734 https://doi.org/10.1061/(asce)gt.1943-5606.0001877
735 Yang, Y. L., K. R. Reddy, Y. J. Du, and R. D. Fan. 2019. "Retention of Pb and Cr (VI)
736 onto slurry trench vertical cutoff wall backfill containing phosphate dispersant

737 amended Ca-bentonite." *Appl. Clay Sci.* 168: 355-365. https://doi.org/
738 10.1016/j.clay.2018.11.023
739 Yi, Y., C. Li, S. Liu, and A. Al-Tabbaa. 2014. "Resistance of MgO–GGBS and
740 CS–GGBS stabilised marine soft clays to sodium sulfate attack." *Géotechnique*.
741 64(8): 673-679. https://doi.org/10.1680/geot.14.t.012
742 Young, Jo. H., C. H. Benson, and T. B. Edil. 2004. "Hydraulic conductivity and
743 cation exchange in non-prehydrated and prehydrated bentonite permeated with weak
744 inorganic salt solutions." *Clay Clay Min.* 52(6): 661-679.
745 https://doi.org/10.1346/ccmn.2004.0520601
746 Zhou, A., R. Huang, and D. Sheng. 2016. "Capillary water retention curve and shear
747 strength of unsaturated soils." *Can. Geotech. J.* 53(6): 974-987.
748 https://doi.org/10.1139/cgj-2015-0322
749

Table

Table 1. Physicochemical properties of the sandy-clay and bentonite

Index	Values		Testing method
	clayey sand	bentonite	
Moisture, (%)	4.81	11.2	(ASTM 2010a)
pH	7.32	8.6	
Specific gravity, G_s	2.62	2.66	(ASTM 2014)
Plastic limit, w_P (%)	-	55	(ASTM 2010b)
Liquid limit, w_L (%)	-	103	(ASTM 2010b)
Grain size distribution (%)			(ASTM 2010c)
Clay (<0.002 mm) [a]	5.62	99	
Silt (0.002-0.075 mm) [a]	14.18	1	
Sand (0.075-2 mm) [b]	80.20	-	
Total surface area, SSA (m^2/g) [c]	-	378.5	
Exchangeable cation (cmol/kg)			(ASTM 2010c)
Ca^{2+}		22.74	
Mg^{2+}		1.41	
Na^{+}		53.39	
K^{+}		0.53	
Sum		78.07	

[a] Measured using a laser particle analyzer Mastersizer 2000 (Malvern Instruments Ltd., UK)

[b] Measured with standard #10 - #200 sieves

[c] Measured using the EGME methods according to (Cerato and Lutenegger 2002).

Table 2. Chemical compositions of clayed sand, OPC, GGBS and MgO by X-ray fluorescence

Oxide Chemistry	Clayey sand (%)	OPC (%)	GGBS (%)	MgO (%)
CaO	0.41	49.75	34.00	0.23
Al_2O_3	35.76	10.87	17.90	0.28
MgO	0.06	2.26	6.02	92.95
K_2O	0.15	0.75	0.64	0.01
SiO_2	48.73	22.6	34.3	0.28
Fe_2O_3	6.13	3.50	1.02	-
SO_3	0.07	3.84	1.64	0.45
MnO	0.11	0.24	0.28	0.01
Loss of ignition (%)	8.58	6.19	4.20	5.79

Table 3. Codification of investigated mix proportions (by unit weight of clayey sand, %)

Category ID	Code	Clayey sand	Bentonite	OPC	GGBS	MgO
Ref	Ref	100	-	5	-	-
CB	C5B5	100	5	5	-	-
	C10B10	100	10	10	-	-
CSB	CS5B5	100	5	1	4	-
	CS10B10	100	10	2	8	-
MSB	MS5B5	100	5	-	4.5	0.5
	MS5B10	100	10	-	4.5	0.5
	MS5B15	100	15	-	4.5	0.5
	MS10B10	100	10	-	9	1
	MS10B15	100	15	-	9	1

Table 4. Summarization of fitting equations, moisture and density for fresh backfills

Code	S_s = aw-b			Measured standard slump (mm)	Measured mini-slump (mm)	Measured water content[a], w (%)	Dry density[b], ρ (g/cm^3)	Void ratio[c], (e)
	a	b	R^2					
Ref	31.6	410	0.99	146	48.3	17.5	1.42	0.84
C5B5	14.4	188	0.99	146	48.6	23.2	1.40	0.88
C10B10	11.7	251	0.97	149	50.0	34.0	1.38	0.89
CS5B5	13.1	154	0.95	146	48.5	23.1	1.43	0.84
CS10B10	24.0	554	0.99	150	50.5	29.3	1.42	0.87
MS5B5	27.9	516	0.96	152	51.5	23.9	1.42	0.85
MS5B10	27.3	765	0.98	154	52.3	33.6	1.36	0.93
MS5B15	26.0	975	0.97	152	51.3	34.7	1.36	0.95
MS10B10	29.2	882	0.98	153	52.4	35.4	1.37	0.94
MS10B15	26.3	807	0.96	155	52.6	36.5	1.36	0.94

[a] ASTM D2216 (ASTM 2010a)

[a] ASTM D7263(ASTM 2018b)

[c] Void ratio (e) determined by water content with the expression $e = G_s \times \rho_w / \rho_d - 1$, where G_s is the specific gravity of backfills, w is the water content, ρ_w and ρ_d are the density of water and dry density of backfills, respectively.

21 **Table 5. Summation of dry density (g/cm^3) and void ratio for aged backfills**

Code	Dy density (g/cm^3)			void ratio (*e*)		
Curing time	0 day	28 days	90 days	0 day	28 days	90 days
Ref	1.43	1.44	1.44	0.84	0.82	0.82
C5B5	1.40	1.41	1.42	0.88	0.87	0.85
C10B10	1.37	1.38	1.39	0.89	0.89	0.89
CS5B5	1.42	1.43	1.43	0.84	0.84	0.83
CS10B10	1.41	1.42	1.43	0.87	0.87	0.85
MS5B5	1.40	1.41	1.43	0.89	0.87	0.85
MS5B10	1.36	1.39	1.41	0.93	0.90	0.87
MS5B15	1.35	1.38	1.41	0.95	0.92	0.88
MS10B10	1.36	1.38	1.40	0.94	0.92	0.89
MS10B15	1.36	1.38	1.40	0.94	0.92	0.89

22

Table 6. Breakdown of embodied CO_2 emission and materials cost for cutoff wall Component

Component	CO_2 emission (kg/t)	Cost (USD/t)
OPC	870-940[a]	78[f]
GGBS	0.143[b]	54[f]
MgO	1400[c]	90[f]
Bentonite	0.05[d]	55[f]
Water	< 0.001	1[f]

[a] Data from Pacheco-Torgal et al., 2017

[b] Data from Heidrich et al. 2005

[c] Data from Mo et al. 2017

[d] Data from USEPA (1994)

[f] Average market price in Nanjing city (China) (2018)

Table 7. Comparison of CO_2 emission and materials cost for the cutoff wall backfills

Code	Net CO_2 emission (kg/m^3)	Costs (USD/m^3)
Ref	54.3	4.7
C5B5	48.4	7.2
C10B10	80.7	11.8
CS5B5	10.0	6.3
CS10B10	17.2	10.7
MS5B5	7.4	6.1
MS5B10	6.3	7.7
MS5B15	5.6	9.2
MS10B10	12.0	9.8
MS10B15	11.5	11.5

Figure 1

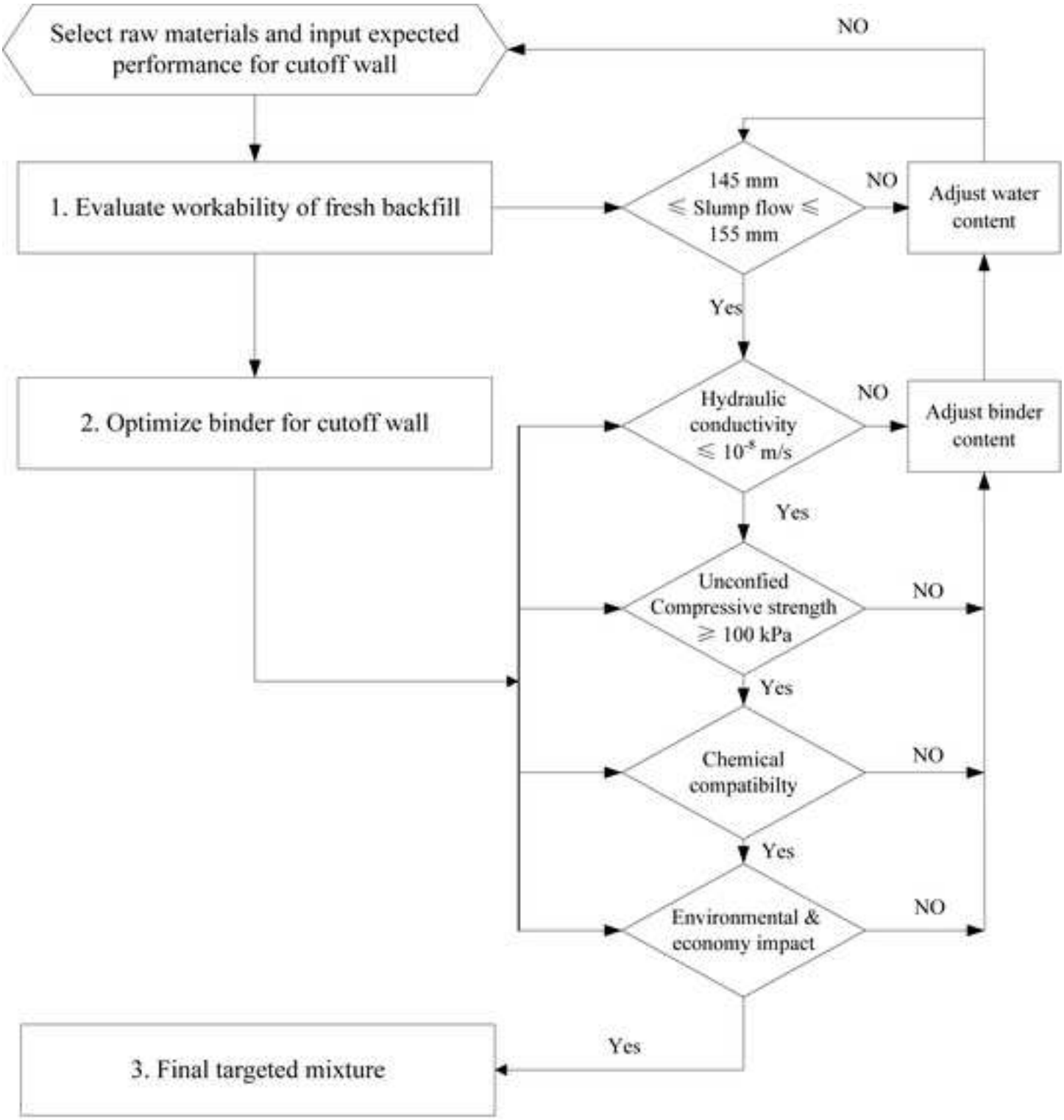
Select raw materials and input expected performance for cutoff wall
NO
1. Evaluate workability of fresh backfill
145 mm ⩽ Slump flow ⩽ 155 mm
NO
Adjust water content
Yes
2. Optimize binder for cutoff wall
Hydraulic conductivity ⩽ 10^{-8} m/s
NO
Adjust binder content
Yes
Unconfied Compressive strength ⩾ 100 kPa
NO
Yes
Chemical compatibilty
NO
Yes
Environmental & economy impact
NO
Yes
3. Final targeted mixture

Figure 2(a)

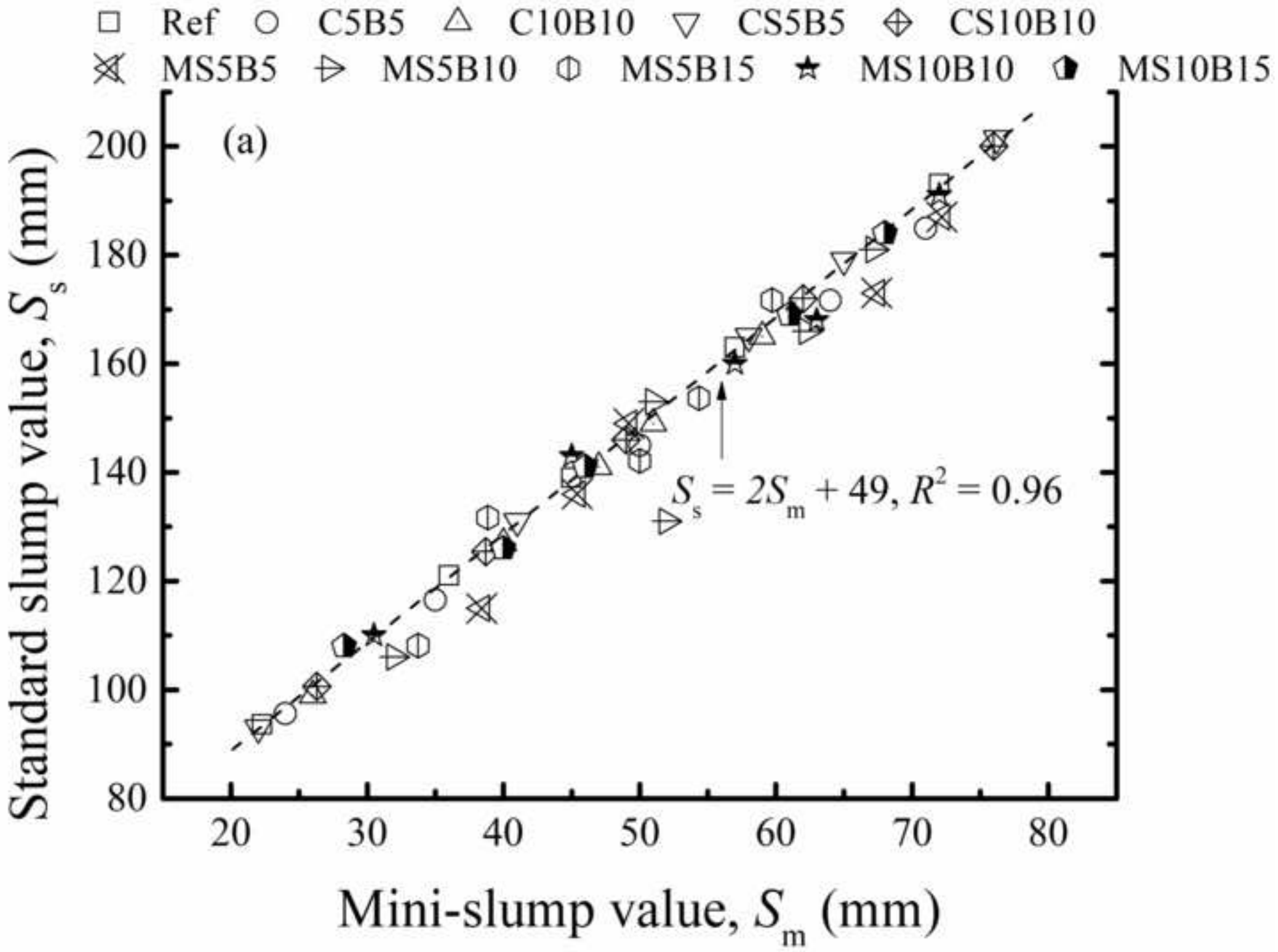
Ref
C5B5
C10B10
CS5B5
CS10B10
MS5B5
MS5B10
MS5B15
MS10B10
MS10B15
(a)
$S_s = 2S_m + 49, R^2 = 0.96$
Standard slump value, S_s (mm)
Mini-slump value, S_m (mm)
200
180
160
140
120
100
80
20
30
40
50
60
70
80

Figure 2(b)

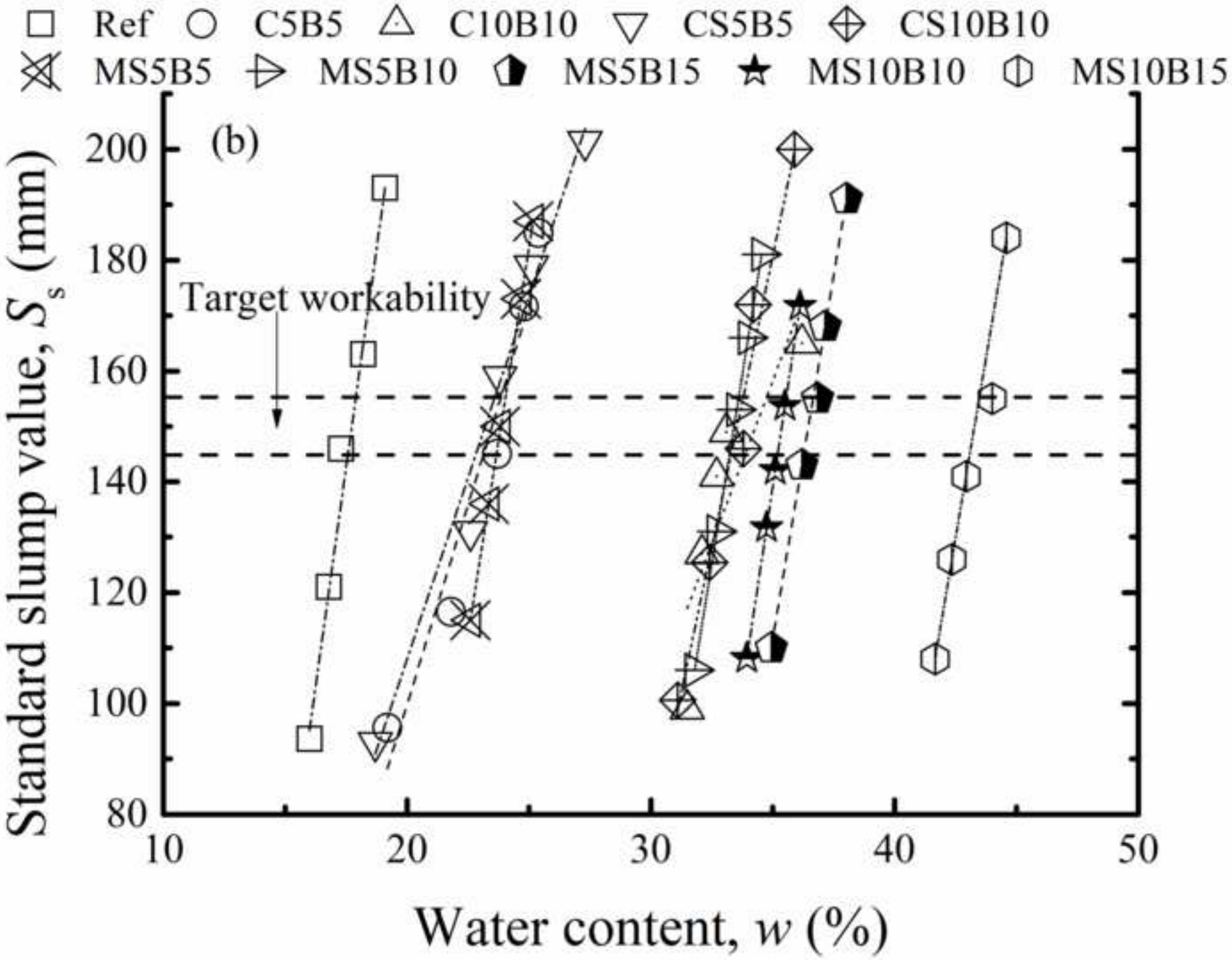
Ref
C5B5
C10B10
CS5B5
CS10B10
MS5B5
MS5B10
MS5B15
MS10B10
MS10B15
(b)
Target workability
Standard slump value, S_s (mm)
Water content, w (%)
200
180
160
140
120
100
80
10
20
30
40
50

Figure 3(a)

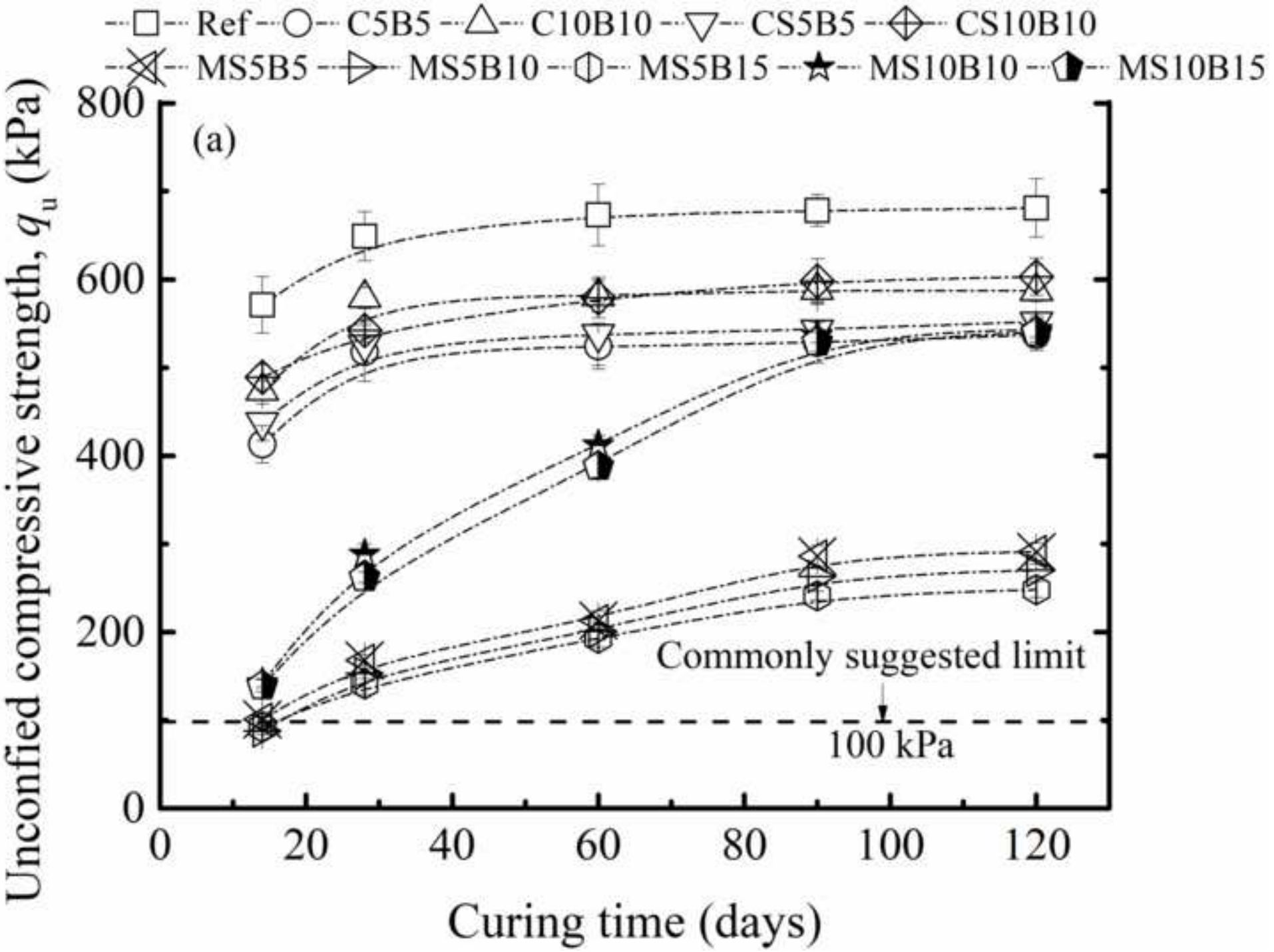
Ref
C5B5
C10B10
CS5B5
CS10B10
MS5B5
MS5B10
MS5B15
MS10B10
MS10B15
(a)
Unconfied compressive strength, q_u (kPa)
800
600
400
200
0
0
20
40
60
80
100
120
Curing time (days)
Commonly suggested limit
100 kPa

Figure 3(b)

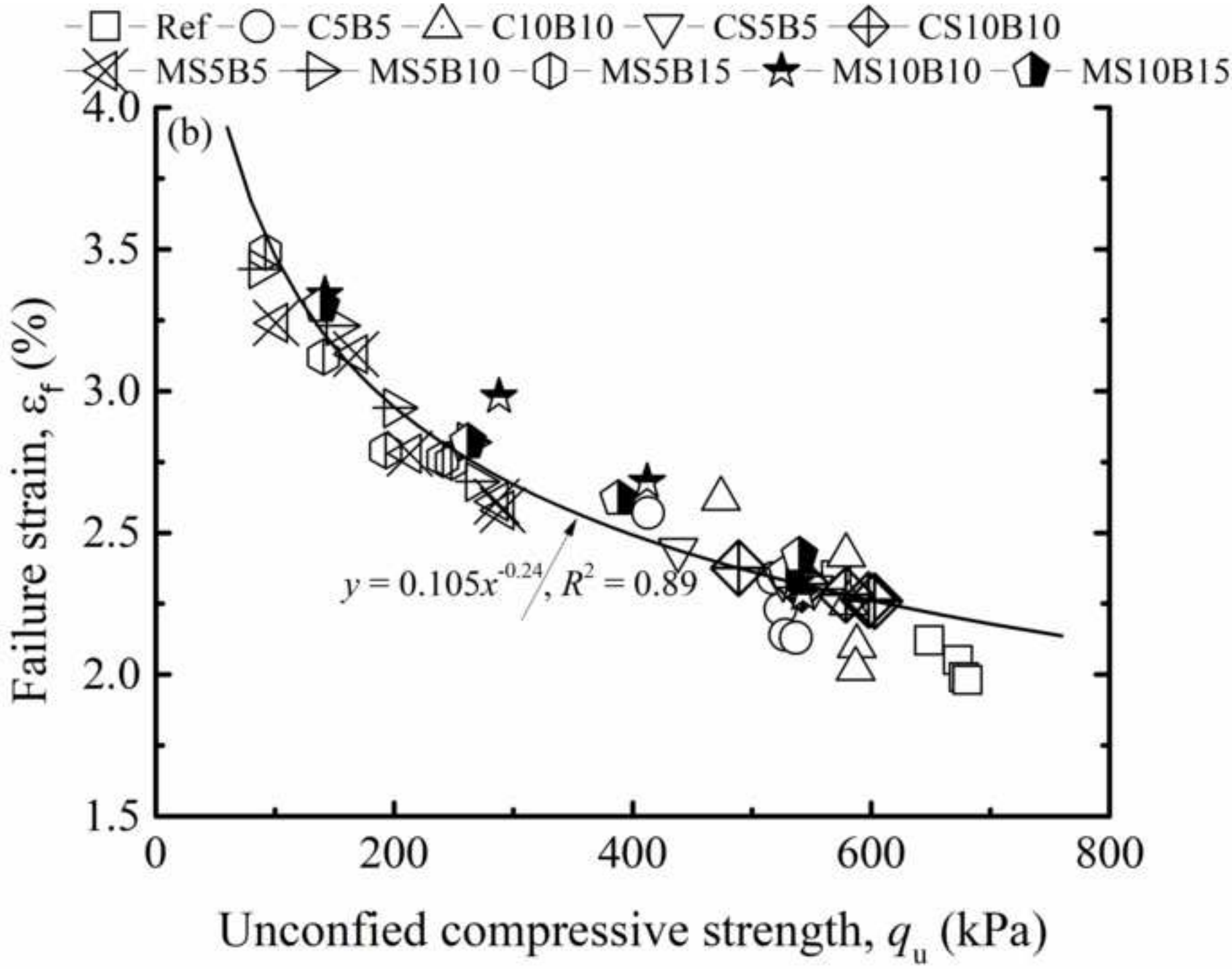
Ref
C5B5
C10B10
CS5B5
CS10B10
MS5B5
MS5B10
MS5B15
MS10B10
MS10B15
(b)
$y = 0.105x^{-0.24}$, $R^2 = 0.89$
Failure strain, ε_f (%)
Unconfied compressive strength, q_u (kPa)
4.0
3.5
3.0
2.5
2.0
1.5
0
200
400
600
800

Figure 4

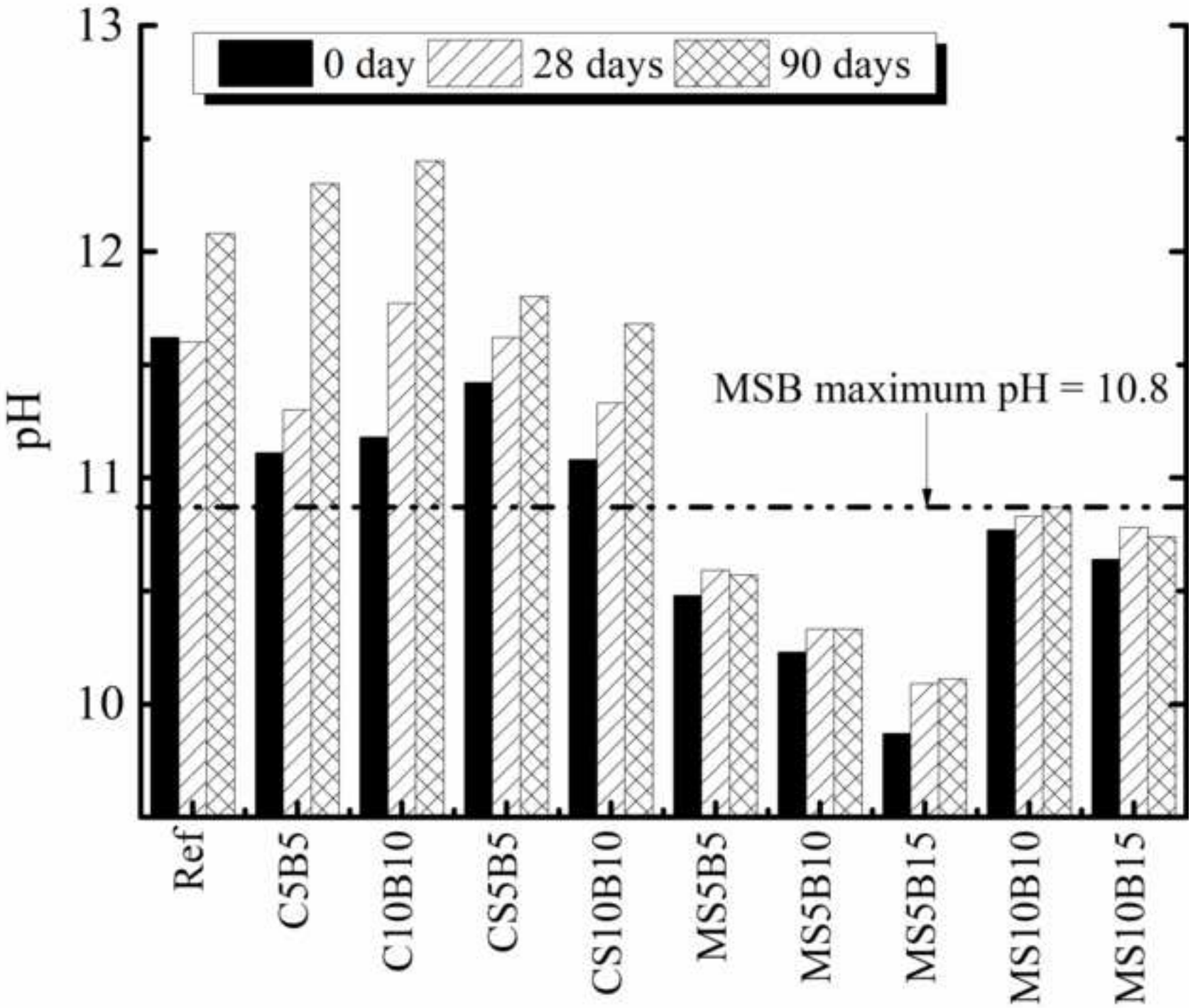
13
12
11
10
pH
0 day
28 days
90 days
MSB maximum pH = 10.8
Ref
C5B5
C10B10
CS5B5
CS10B10
MS5B5
MS5B10
MS5B15
MS10B10
MS10B15

Figure 5

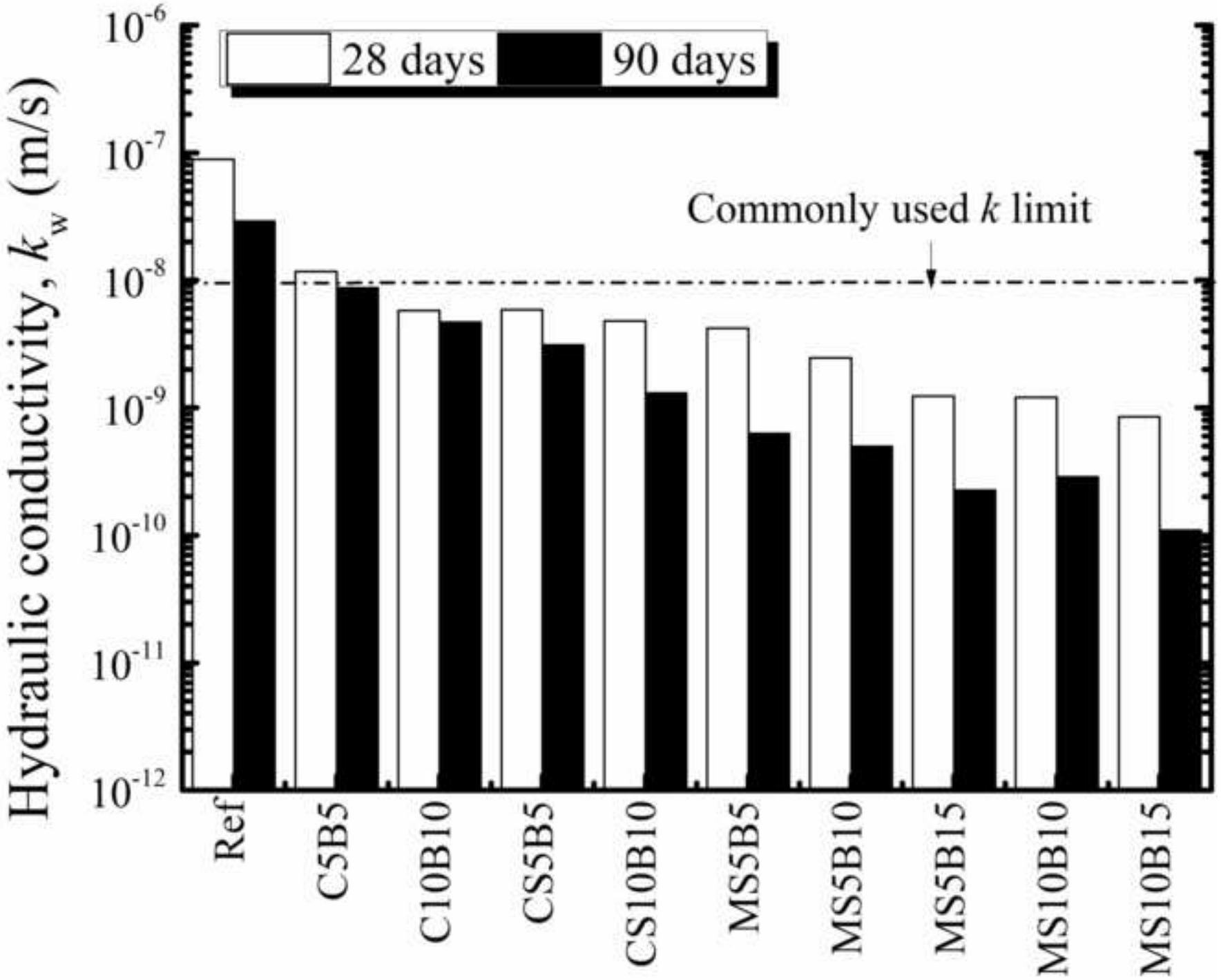
Hydraulic conductivity, k_w (m/s)
10^{-6}
10^{-7}
10^{-8}
10^{-9}
10^{-10}
10^{-11}
10^{-12}
28 days
90 days
Commonly used k limit
Ref
C5B5
C10B10
CS5B5
CS10B10
MS5B5
MS5B10
MS5B15
MS10B10
MS10B15

Figure 6(a)

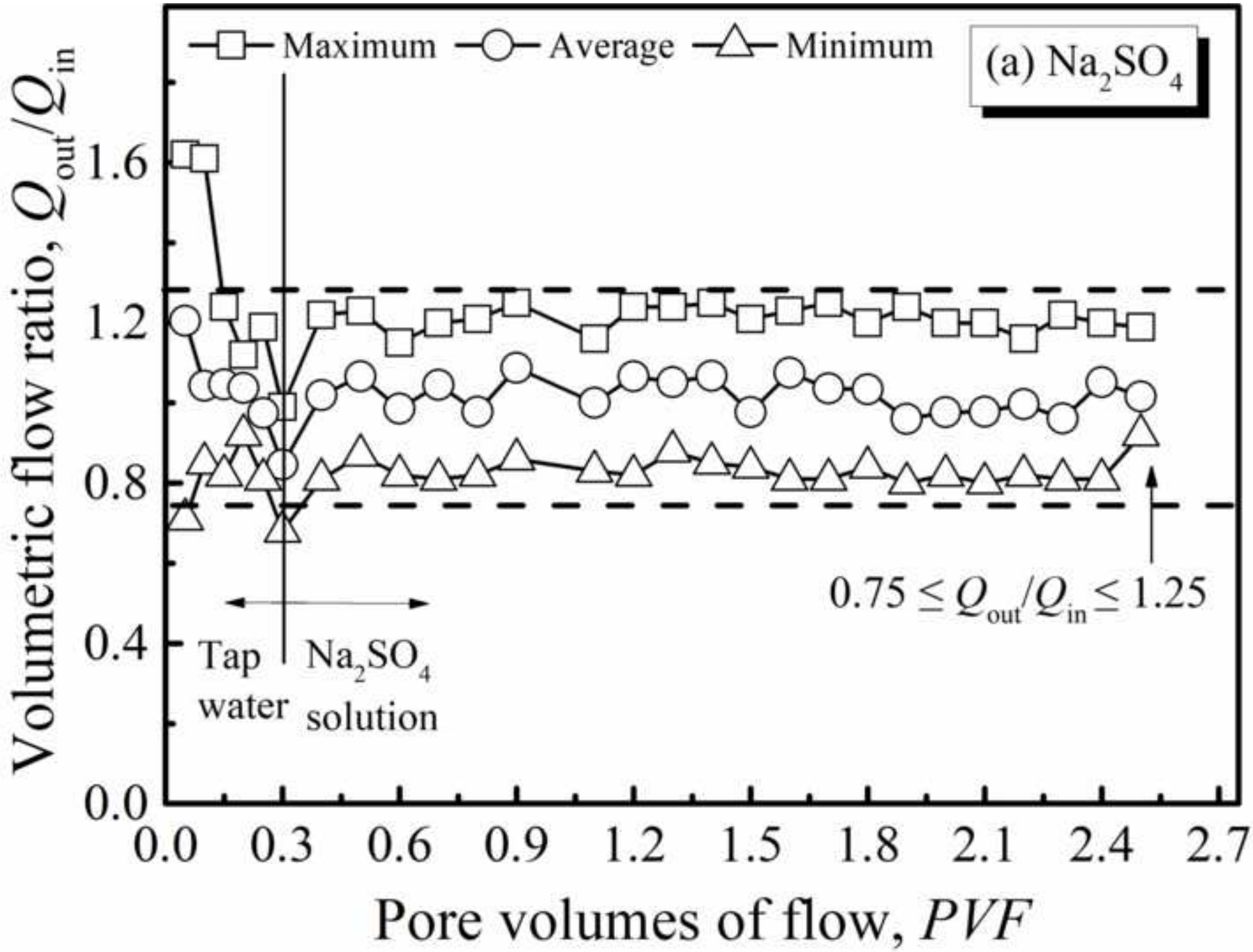
Maximum
Average
Minimum
(a) Na_2SO_4
Volumetric flow ratio, Q_{out}/Q_{in}
1.6
1.2
0.8
0.4
0.0
$0.75 \le Q_{out}/Q_{in} \le 1.25$
Tap water
Na_2SO_4 solution
0.0
0.3
0.6
0.9
1.2
1.5
1.8
2.1
2.4
2.7
Pore volumes of flow, *PVF*

Figure 6(b)

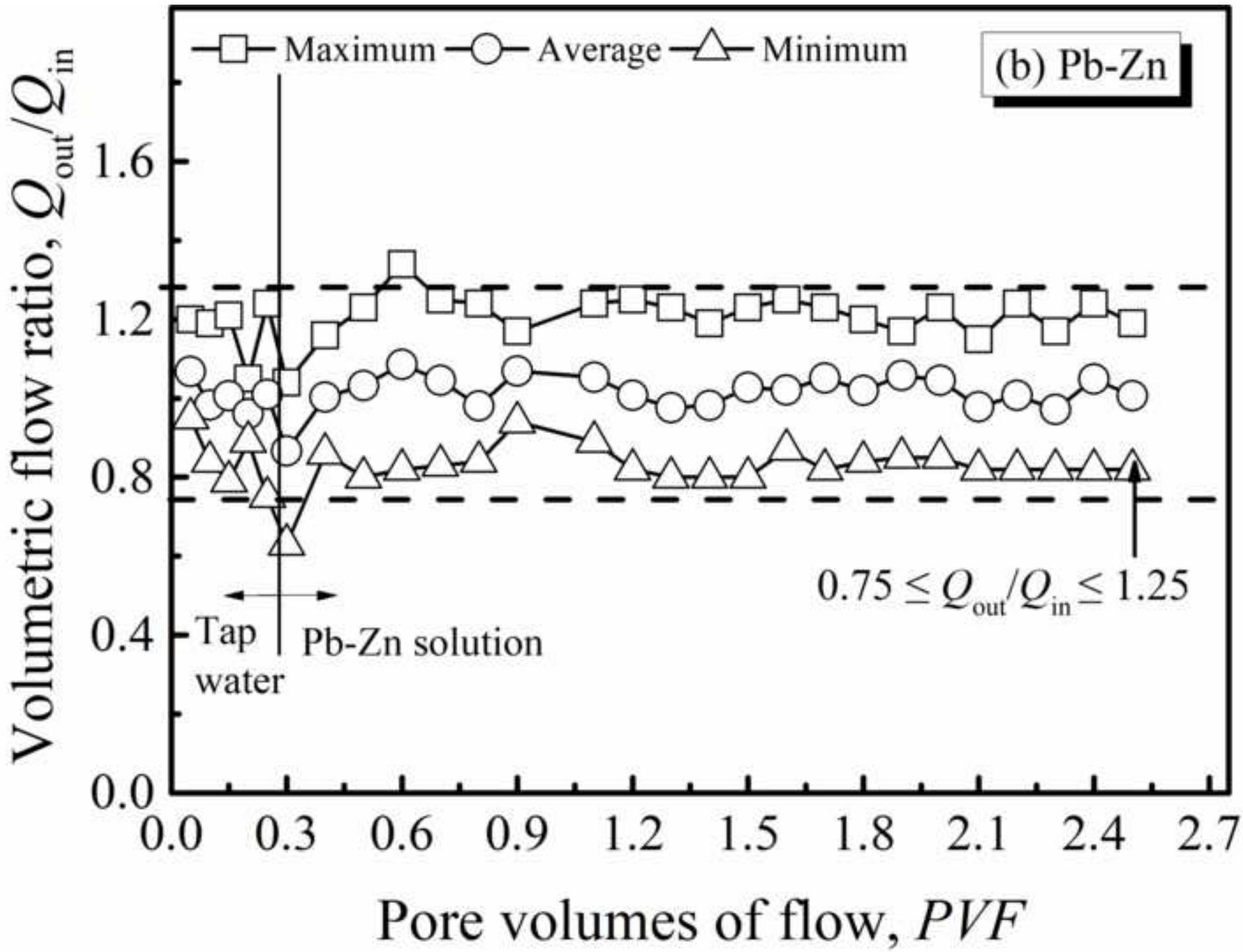
Maximum
Average
Minimum
(b) Pb-Zn
Volumetric flow ratio, Q_{out}/Q_{in}
1.6
1.2
0.8
0.4
0.0
$0.75 \leq Q_{out}/Q_{in} \leq 1.25$
Tap water
Pb-Zn solution
0.0
0.3
0.6
0.9
1.2
1.5
1.8
2.1
2.4
2.7
Pore volumes of flow, *PVF*

Figure 6(c)

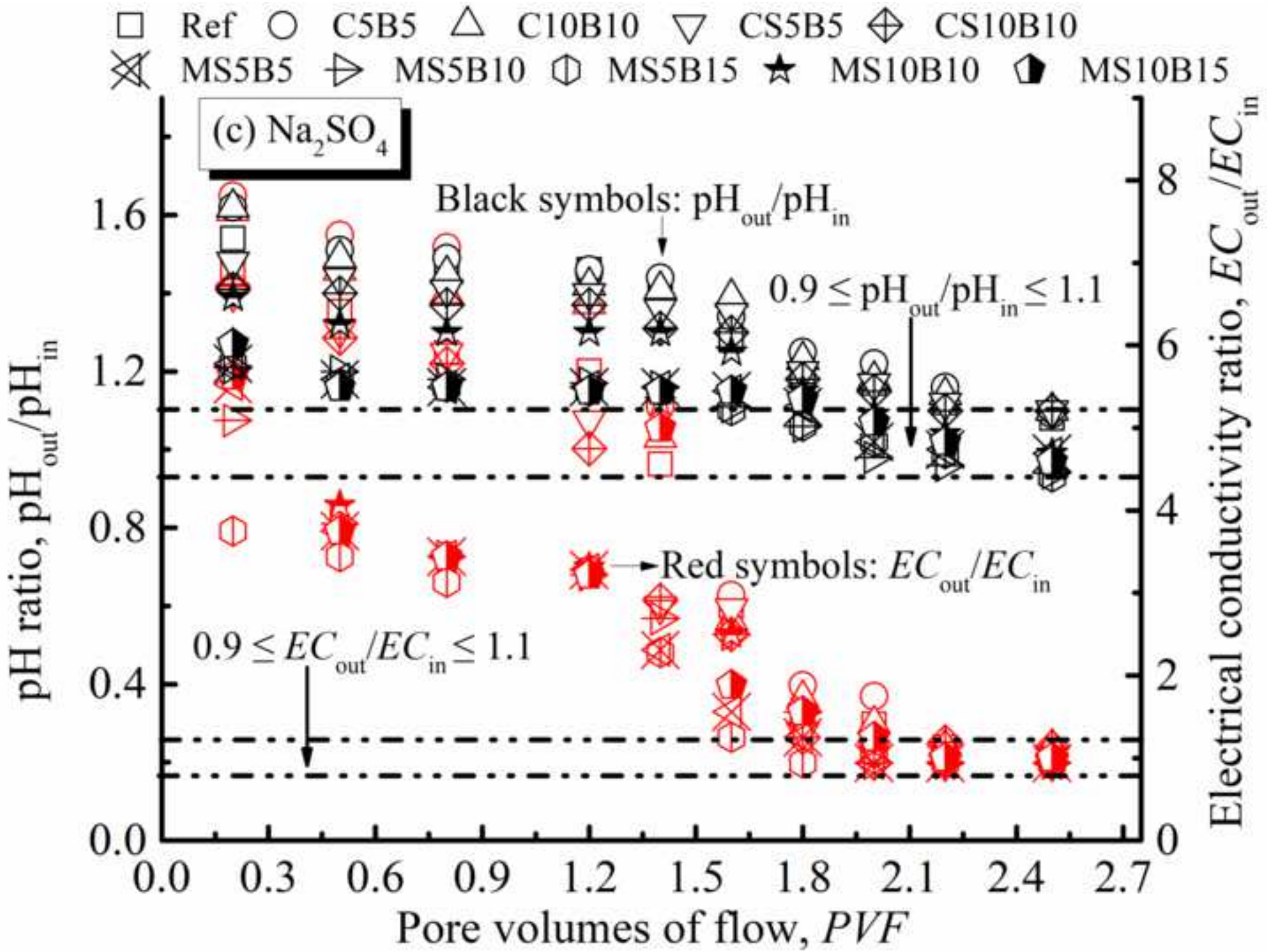
Ref
C5B5
C10B10
CS5B5
CS10B10
MS5B5
MS5B10
MS5B15
MS10B10
MS10B15
(c) Na2SO4
Black symbols: pHout/pHin
0.9 ≤ pHout/pHin ≤ 1.1
Red symbols: ECout/ECin
0.9 ≤ ECout/ECin ≤ 1.1
pH ratio, pHout/pHin
Electrical conductivity ratio, ECout/ECin
Pore volumes of flow, PVF
0.0
0.4
0.8
1.2
1.6
0
2
4
6
8
0.0
0.3
0.6
0.9
1.2
1.5
1.8
2.1
2.4
2.7

Figure 6(d)

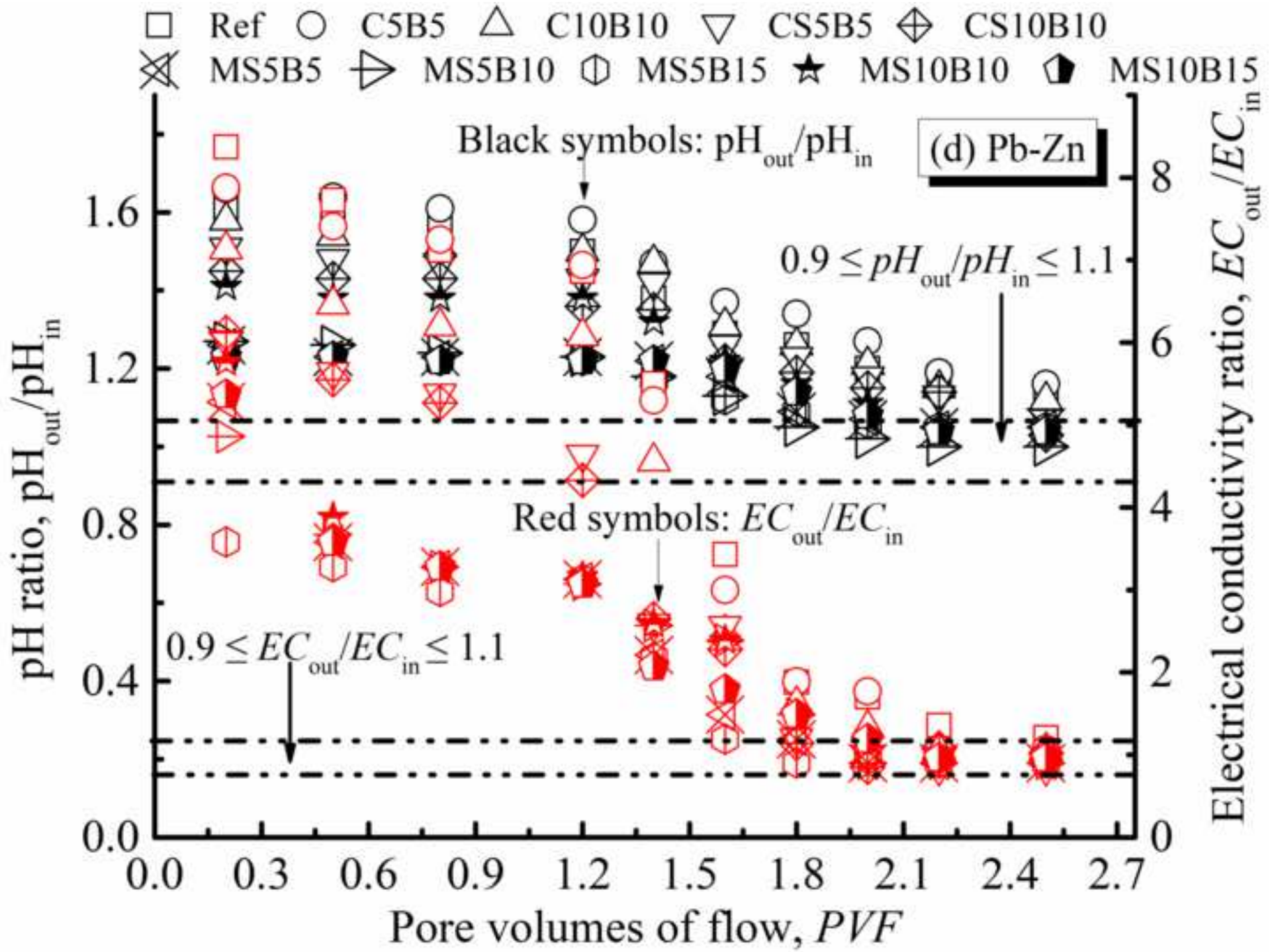
Ref
C5B5
C10B10
CS5B5
CS10B10
MS5B5
MS5B10
MS5B15
MS10B10
MS10B15
Black symbols: pH_{out}/pH_{in}
(d) Pb-Zn
$0.9 \le pH_{out}/pH_{in} \le 1.1$
Red symbols: EC_{out}/EC_{in}
$0.9 \le EC_{out}/EC_{in} \le 1.1$
pH ratio, pH_{out}/pH_{in}
Electrical conductivity ratio, EC_{out}/EC_{in}
Pore volumes of flow, PVF
0.0
0.4
0.8
1.2
1.6
0
2
4
6
8
0.0
0.3
0.6
0.9
1.2
1.5
1.8
2.1
2.4
2.7

Figure 6(e)

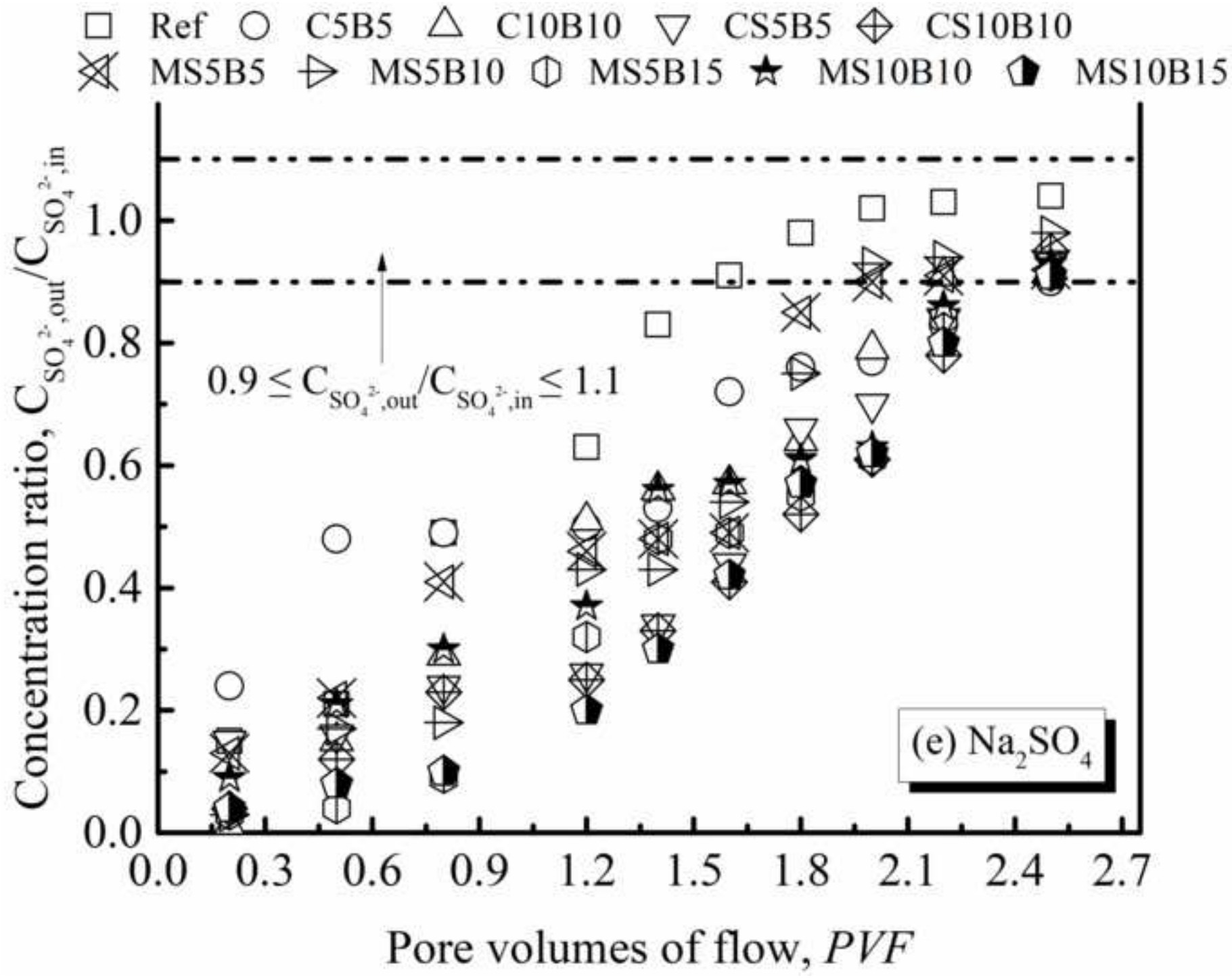
Ref
C5B5
C10B10
CS5B5
CS10B10
MS5B5
MS5B10
MS5B15
MS10B10
MS10B15
Concentration ratio, $C_{SO_4^{2-},out}/C_{SO_4^{2-},in}$
$0.9 \le C_{SO_4^{2-},out}/C_{SO_4^{2-},in} \le 1.1$
(e) Na_2SO_4
0.0
0.2
0.4
0.6
0.8
1.0
0.0
0.3
0.6
0.9
1.2
1.5
1.8
2.1
2.4
2.7
Pore volumes of flow, *PVF*

Figure 6(f)

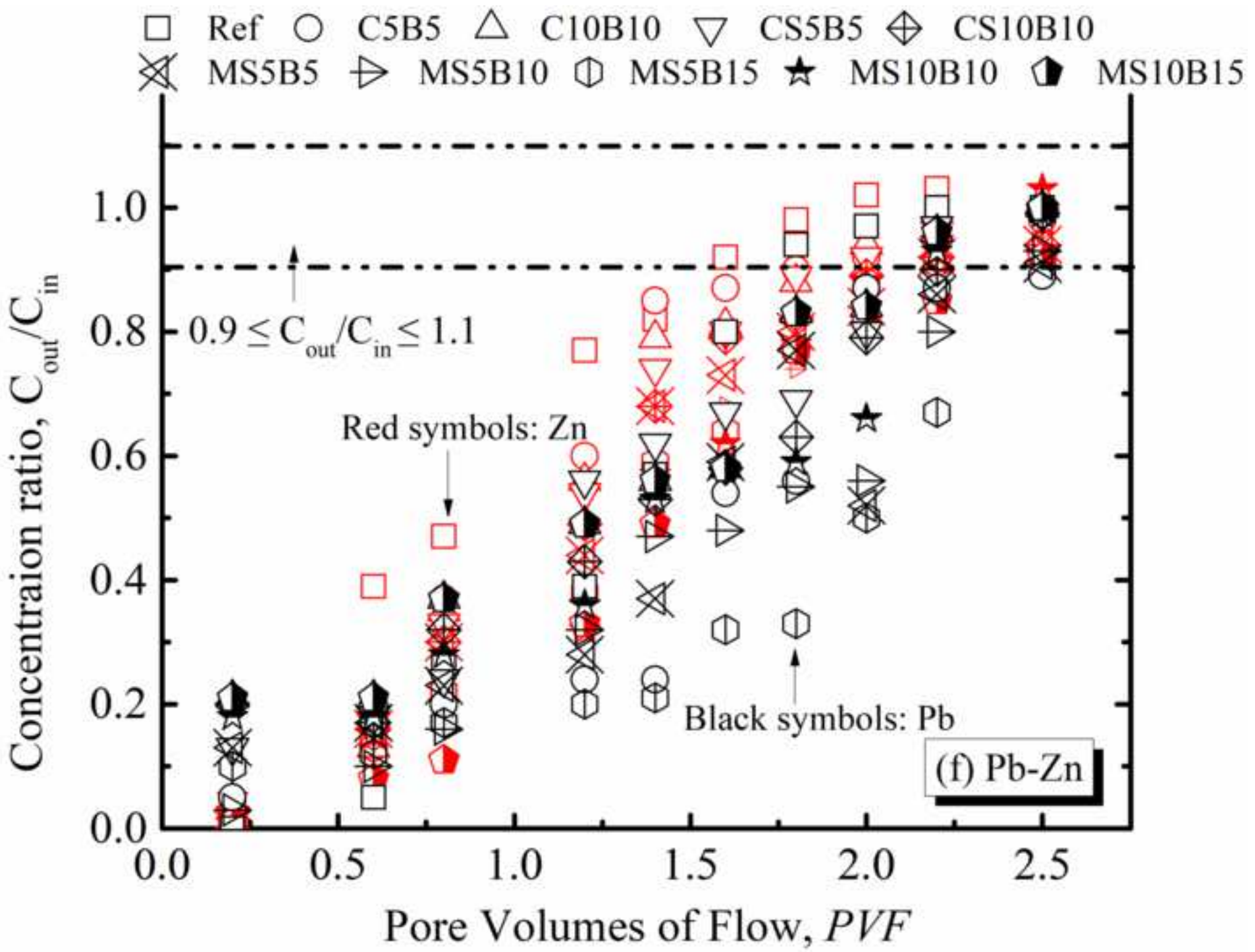
Ref
C5B5
C10B10
CS5B5
CS10B10
MS5B5
MS5B10
MS5B15
MS10B10
MS10B15
0.9 ≤ C_out/C_in ≤ 1.1
Red symbols: Zn
Black symbols: Pb
(f) Pb-Zn
Concentraion ratio, C_out/C_in
Pore Volumes of Flow, PVF
0.0
0.2
0.4
0.6
0.8
1.0
0.0
0.5
1.0
1.5
2.0
2.5

Figure 7

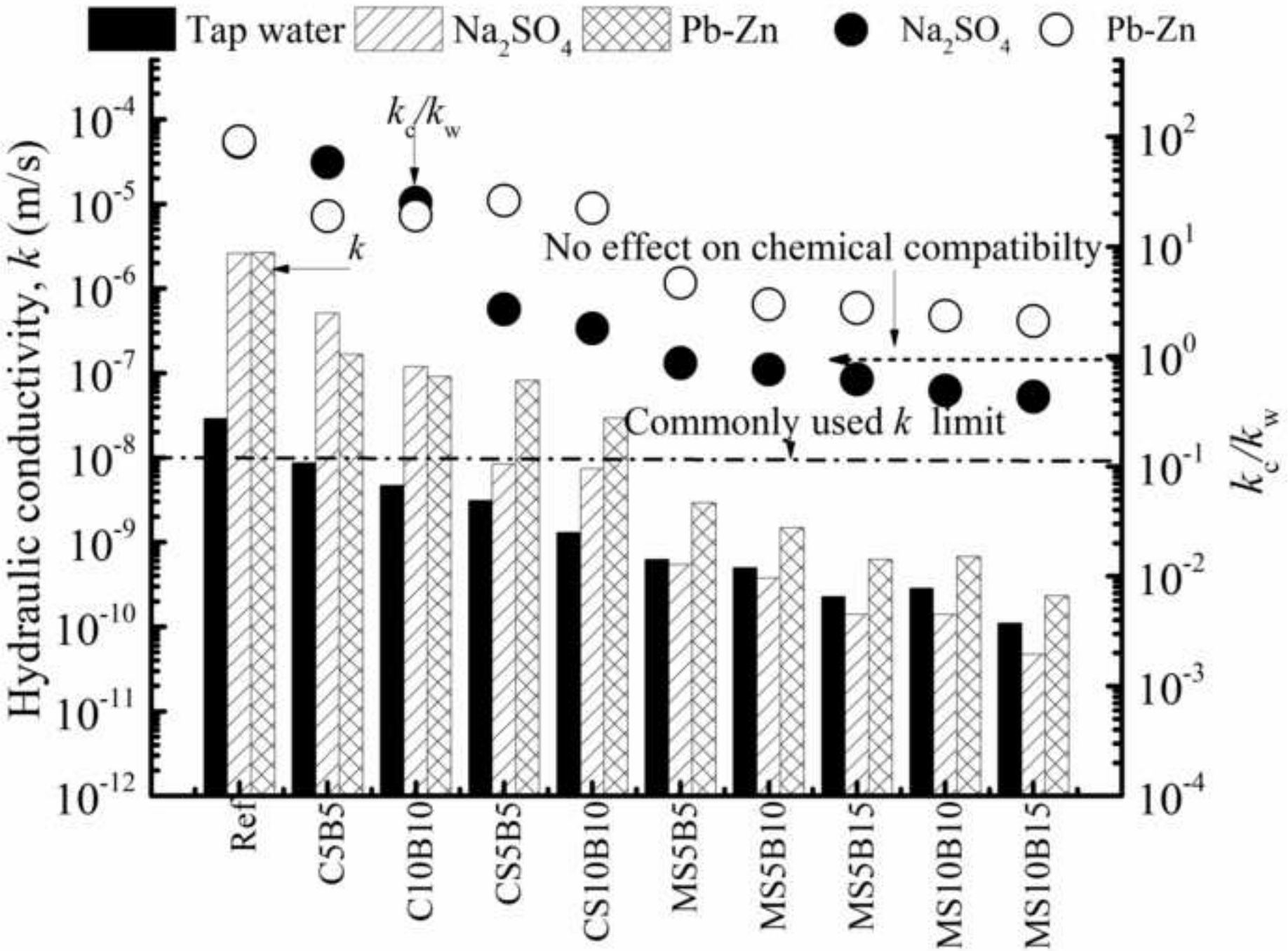
Tap water
Na2SO4
Pb-Zn
Na2SO4
Pb-Zn
Hydraulic conductivity, k (m/s)
kc/kw
k
No effect on chemical compatibilty
Commonly used k limit
kc/kw
Ref
C5B5
C10B10
CS5B5
CS10B10
MS5B5
MS5B10
MS5B15
MS10B10
MS10B15

Table Captions

Figure Captions

Figure 6. Variation of volumetric flow ratio (a and b), pH and *EC* ratio (c and d), and consternation ratio (e and f) with pore volumes of flow (*PVF*) for sodium sulfate and Pb-Zn solution

Figure 7. Measurement of hydraulic conductivity for the cutoff wall specimens exposed to sodium sulfate and Pb-Zn solution